Nanoscale

REVIEW

View Article Online
View Journal | View Issue

Cite this: *Nanoscale*, 2023, **15**, 11313

Recent advances of structural/interfacial engineering for Na metal anode protection in liquid/solid-state electrolytes†

Zirui Yang, Ruijuan Shi, * Zhen Shen and Yong Zhao *

Received 23rd March 2023,
Accepted 14th June 2023

DOI: 10.1039/d3nr01346d

rsc.li/nanoscale

Na metal anode is one of most promising anode materials for next-generation secondary batteries. However, the practical application of Na anode is limited by dendritic growth, rapid volume change, and serious interface problems in the process of Na electroplating/stripping, resulting in low coulombic efficiency, short life, and safety issues of sodium metal batteries (SMBs). Herein, the cyclic instability mechanisms of the Na anode and the corresponding advanced protection strategies including *in situ* solid-electrolyte-interphase (SEI), artificial SEI, and three-dimensional conductive frame, are systematically reviewed. Notably, this review summarizes the latest research progress on interface modification and electrode modification of all-solid-state SMBs. Finally, the outlooks of anode interphase in SMBs are summarized and prospected, providing a promising way for high-energy and safe SMBs.

1. Introduction

In the past decades, the vigorous development of secondary batteries has changed the lifestyle of human society. Since Sony company first commercialized lithium ion batteries (LIBs) in the 1990s, they have become the most common power supply in the portable electronic product market.[1–4] However, due to the large-scale application of LIBs, the demand for the main raw materials has risen sharply, which cannot meet the growing demand and large-scale energy storage equipments.[5,6] In contrast, with the merits of abundant resource and low cost of Na resource, sodium metal batteries (SMBs) are considered as one of the promising alternative to LIBs in the application fields of large scale energy storage grids, low-speed electric vehicles, electric drones, *etc*. For example, not only the cost of Na but also the cost of Al collector in SMBs are much cheaper than those of Li and Cu collector (the price of Al is $ 0.3 per m^2, and the price of Cu is $ 1.2 per m^2) in the lithium metal battery (LMB).

Key Lab for Special Functional Materials of Ministry of Education; National & Local Joint Engineering Research Center for High-efficiency Display and Lighting Technology; School of Materials Science and Engineering; Collaborative Innovation Center of Nano Functional Materials and Applications; Henan University, Kaifeng, 475004, P. R. China. E-mail: 10330121@henu.edu.cn, zhaoyong@henu.edu.cn

† Celebrating the 25th anniversary of the Key Laboratory for Special Functional Materials of Ministry of Education at Henan University.

Zirui Yang

Zirui Yang received his B.S. degree from Henan University, Minsheng College, Kaifeng, in 2021. He is currently a Master's candidate under the supervision of Prof. Yong Zhao at Henan University. His current research mainly focuses on the anode protection strategy for rechargeable sodium metal batteries.

Ruijuan Shi

Ruijuan Shi received her B.S. degree from Henan Normal University, Xinxiang, China, in 2014 and a Ph.D. degree from Nankai University, Tianjin, China, in 2020. She is currently a lecturer at Henan University. Her research interests are focused on the fabrication of advanced electrode materials and electrolyte modification for rechargeable metal batteries.

The ionic radius of Na^+ (1.02 Å) is larger than Li^+ (0.76 Å), which will affect the interphase substance, transport properties, and interphase formation. Compared with Li^+, the larger Na^+ with lower solvation energy undergoes a faster ion transport rate upon Na plating/stripping processes. Once Na is directly deposited on the anode during charging and discharging, rather than in the embedded compounds such as graphite stored in the sodium ion battery, the maximum gravimetric capacity of the battery will be significantly increased. In the field of room temperature SMBs, significant progress has been made in the cathodic side (such as layered oxide materials, polyphosphates, S, and O_2).[7–13] Two types of cathode materials have been developed for SMBs. The first type is intercalated materials such as anionic compounds, layered transition metal oxides, and Prussian blue analogs (PBAs). The intercalated cathode is mostly utilized in high voltage SMBs, although its specific capacity is constrained. The second type is conversion materials that include S, O_2, metal oxides, and sulfides, which always have high specific capacities. For example, the theoretical energy density of the Na–S battery is up to 1274 W h kg^{-1} due to the high capacities of S cathode (1675 mA h g^{-1}) and Na anode (1166 mA h g^{-1}).[14–17]

Compared to the widely investigated cathode materials that also have been successfully applied to sodium ion batteries, the bottleneck on the negative side of SMBs should be paid more attention. Generally, Na anode is slightly irreversible during the repeated plating and stripping due to its high reactivity with the electrolyte. During the process of Na deposition and stripping, Na with high reductive activity easily reacts with electrolyte and forms a solid electrolyte interphase (SEI) on its surface. Notably, the original SEI layer generally experiences the uneven flow of ions and low transfer rate of Na^+ on the Na surface, resulting in the fracture and recombination of SEI films, as well as electrolyte depletion during battery operation.[18–29] Thus, the uneven deposition and stripping of Na surface are easy to cause the growth of Na dendrites and side reactions, leading to low coulombic efficiency (CE), poor stability, and low safety for SMBs. The above issues faced by the Na anode largely limit its practical process in large-scale energy storage systems (Fig. 1). In the past several decades, significant progress has been made in the development of high-performance SMBs. The structural/interfacial engineering on Na metal anode is emerging to regulate Na plating/stripping behavior and improving the cycling stability, while few reviews focus on the interface issues and advanced strategies both in liquid electrolyte and solid-state electrolyte (SSE) of SMBs.[30–34] Moreover, few reviews have related to causes of the key mechanisms behind various issues for Na metal and how to handle electrode/electrolyte interactions in SSEs, which could provide advice and guidance on how to build stable SEI layers in solid-state SMBs.

Herein, we have highlighted the failure mechanisms of the chemical reactions between Na anodes and electrolyte during battery operation, along with advanced strategies (using SEI layer modification and 3D conductive frameworks) to address potential issues about electrode/electrolyte interfaces of SMBs in liquid and SSEs. In this review, we primarily discussed the instability mechanism of Na electrode during cell cycling, which is mainly due to the side reaction and dendrite growth on the surface of Na metal. According to the failure mechanism, this review has elaborated the Na protection strategies from three aspects: *in situ* SEI layer, artificial (*ex situ*) SEI layer, and three-dimensional (3D) frame structure. Notably, the advanced optimization strategies of electrolyte-electrode interface and electrolyte structures in SSE systems are discussed to deal with the poor interface compatibility and slow ion transport problems of SSEs. The electrochemical and chemical behavior of SMBs changes greatly in complex charge/discharge process, which will be reflected in this review. Furthermore, the prospects and challenges of developing high-stable Na anodes are comprehensively presented as well, which provides a promising way to achieve high-energy and safe SMBs in varied applications.

Zhen Shen

Zhen Shen received her B.S. degree from Jining University, in 2021. She is a Master's candidate under the supervision of Prof. Yong Zhao and Lecturer Ruijuan Shi of Henan University. Her current research direction mainly focuses on the application of novel organic materials in secondary batteries.

Yong Zhao

Yong Zhao received his PhD in Physical Chemistry from Institute of Chemistry, Chinese Academy of Sciences in 2008 under the supervision of Prof. Lei Jiang. After that, he joined as a postdoctoral fellow with Prof. Kazuhito Hashimoto in Applied Chemistry at the University of Tokyo (2008–2015). He became a full professor at Henan University in 2016. His research focuses on the mechanism of electrocatalytic reactions and catalyst innovation in fuel cells and advanced materials for rechargeable battery.

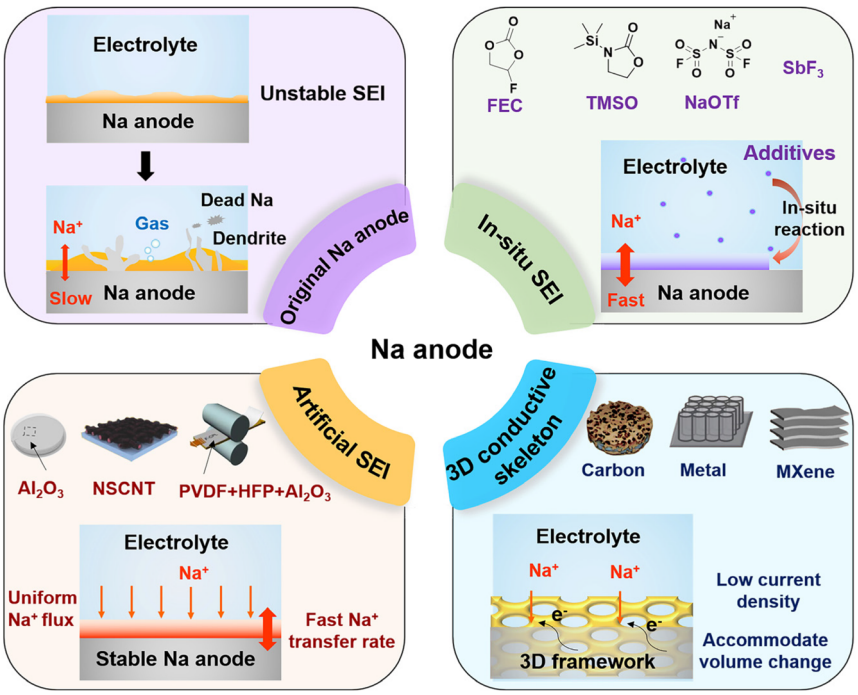

Fig. 1 Primary problems and corresponding solutions of Na anodes.[30,31,151,193,198] (Reprinted with permission from ref. 30, 31, 151, 193 and 198. Copyright 2017 American Chemical Society, Copyright 2018 WILEY-VCH, Copyright 2017 WILEY-VCH, Copyright 2016 WILEY-VCH, and Copyright 2018 WILEY-VCH).

2 Primary problems of SMBs

The direct utilization of Na metal as the anode is likely to offset the advantages of SMBs, especially in traditional liquid electrolytes. Na metal anodes with high chemical reactivity face issues of continuous side reactions, serious Na dendrite growth, and uncontrollable volume expansion during Na deposition process, which leads to inferior cycle life, increased internal polarization, and low CE of SMBs. Battery failures have a close relationship with the Na deposition behaviors, ion flux distribution, and the effect of anode-electrolyte interface on the anode surface; thus it is crucial to figure out the failure mechanisms of the aforementioned issues in view of the future commercialization of high-energy-density SMBs. Here, the detailed issues and related failure mechanisms of Na anodes are discussed as follows.

2.1 Side reactions and the failure mechanism of Na anode

Na has a lower initial ionization energy (495.8 kJ mol^{-1}) than that of Li, and its outermost electrons are simpler to liberate, making it easier to react with the electrolyte and produce substantial self-discharge in the battery. When the lowest unoccupied molecular orbital (LUMO) energy level of electrolyte components is lower than that of Na anode (Fig. 2a), the electrolyte will react with Na metal to generate solid products, which is also called SEI.[35] As a result, Na metal with high reactivity is likely to react with active intermediates in the electrolyte, forming an original SEI layer on the Na metal surface. The unstable SEI raises the internal resistance, side reactions, and Na dendrite growth, leading to the low CE, poor cycling stability, and safety issues of SMBs.

The side reactions between Na and traditional liquid electrolytes are inevitable without SEI modification, even worse in ester-based electrolytes. For example, Ponrouch's research showed that the main components of the SEI layer contained inorganic components (Na_2CO_3) and organic components (RCOONa and HCOONa) in carbonate ester-based electrolytes.[36] As shown in Fig. 2b, the Li/Li symmetrical cell with $LiPF_6$ ethylene carbonate (EC)/dimethyl carbonate (DMC) electrolyte showed fairly steady plating/stripping behavior at a current density of 5 mA cm^{-2}. In contrast, the Na/Na symmetrical cell in the $NaPF_6$ EC/DMC electrolyte exhibited extremely unstable cycling performance, demonstrating poor interface compatibility between Na metal and carbonate ester-based electrolytes. Moreover, impedance testing revealed the continuous reactions between Na and ester-based electrolyte, resulting in a gradual rise in the interface resistance of Na/Na symmetrical cell under open circuit conditions.

Considering the high reactivity of Na metal, it is easy to react with active intermediates in the electrolyte to produce several side reactions, which is usually accompanied by gas evolution as well. For instance, Mullins' team reported that the deposition of Na metal in ester-based electrolytes (the hybrid of EC, diethyl carbonate (DEC), and PC) can produce a large amount of gas and fragile porous dendrites (Fig. 3a–f).[37,38] The addition of fluoroethylene carbonate (FEC) solvent in DEC significantly reduced gas emissions during Na deposition, demonstrating that the formation of a dense SEI layer could

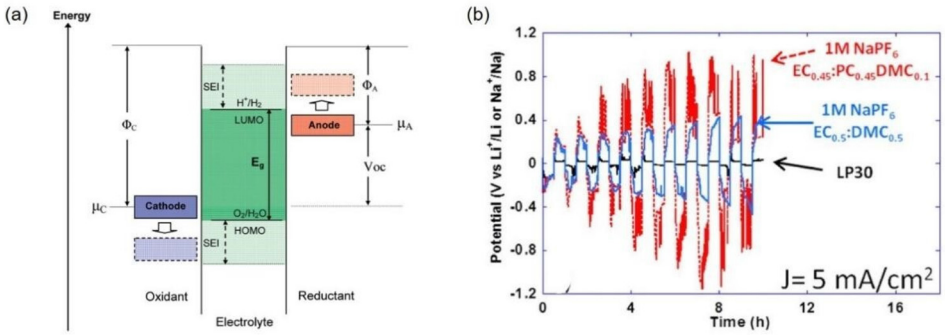

Fig. 2 (a) Schematic relative electron energies map of electrodes and the electrolyte in a stable battery.[35] (b) For the circulation of Li/Li and Na/Na symmetrical batteries in LP30 at 25 °C, 1 M $NaPF_6$ is added in $EC_{0.5}DMC_{0.5}$ or 1 M $NaPF_6$ is added in $EC_{0.45}PC_{0.45}DMC_{0.1}$, and the current density was 5 mA cm^{-2}.[36] (Reprinted with permission from ref. 35 and 36. Copyright 2009 American Chemical Society and Copyright 2015 Electrochemical Society).

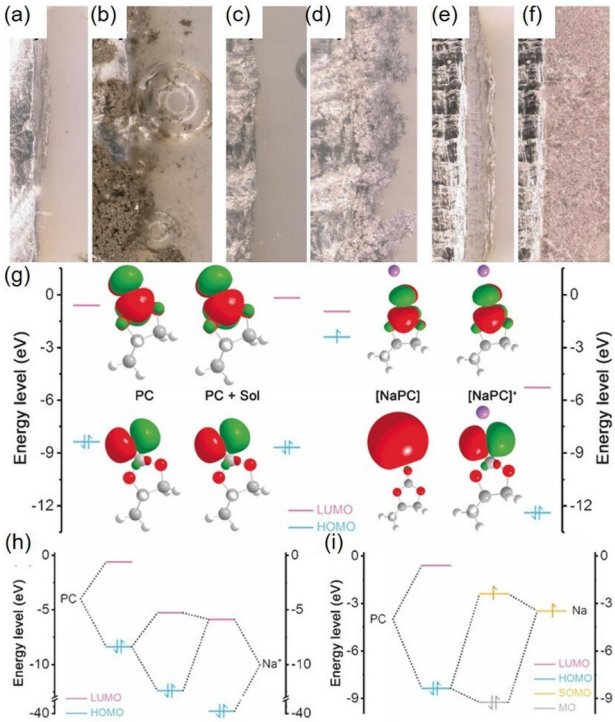

Fig. 3 All images corresponding to Na matrix before and after deposition in the (a and b) EC/DEC, (c and d) PC/FEC, and (e and f) FEC/DEC/DEC electrolytes. (g) Frontier molecular orbital theory analysis.[37] The frontier molecular orbital level of PC (single PC molecule), PC + Sol (PC molecule considering solvent effect), [NaPC] (Na atom PC complex), and $[NaPC]^+$ (Na^+ ion PC complex). H, Li, C, and O atoms were marked in white, purple, gray, and red, respectively. Schematic diagram of orbital hybridization between PC and (h) Na ion and (i) Na atom.[39] (Reprinted with permission from ref. 37 and 39. Copyright 2014 American Chemical Society and Copyright 2018 WILEY-VCH).

prevent further decomposition of the FEC/DEC (1 : 1 volume) electrolyte and improve the cycling stability of Na metal anode. The rigid-shelled button batteries are insensitive to gas generation, while it is crucial to research the gas generation in pouch-type cells. Zhang *et al.* reported that the ion-solvent complexes with lower LUMOs (*vs.* pure PC solvent) in the $NaClO_4$/PC electrolyte were prone to react with Na metal, leading to serious electrolyte depletion and gas evolution (Fig. 3g–i).[39] Once PC complexed with Na^+, the LOMO level of the resultant Na^+–PC complex was reduced to −5.28 eV, accompanied by the intense gas generation on the surface of Na metal. Except for the serious side reactions between Na anode and ester-based electrolytes, Cui and colleagues uncovered that ether-based electrolytes with $NaPF_6$ could enable Na anode with highly reversible and nondendritic stripping/plating behavior owing to the impermeable and even inorganic SEI made of NaF and Na_2O.[53] However, ether-based electrolytes electrochemical with narrow electrochemical windows cannot endure long-term exposure to high-voltage and high-temperature testing, causing undesirable electrolyte depletion and evolution of flammable gas on Na anode under extreme conditions.[199] Moreover, ionic liquids and high concentration electrolytes have both been explored in addition to the conventional ester and ether electrolytes used in SMBs, providing steady high voltage performance and a sizable suppression of Na dendrites.

To sum up, highly reactive Na metal is prone to lose the outermost electrons and then react with the electrolyte, thus affecting the Na deposition and evolution behavior and cycling stability of SMBs. The generation mechanism of side reactions is not solitary, and it is closely linked to unstable SEI and Na dendritic growth. The formation of porous Na dendrites increases the contact area between the Na anode surface and the electrolyte, which intensifies the side reactions and gas generation problems. As a result, the gas evolution process must be addressed from the standpoint of the overall SMBs as well as must cope with unstable SEI and Na dendritic formation problems.

2.2 Na dendrite growth and mechanism

An unstable SEI layer is usually correlated with the uneven flux of ions and slow Na^+ transfer rate on a portion of Na surface, resulting in Na dendrite growth and continuous side reactions during the battery operation. Reducing the amount of Na dendrites created during the SMBs cycling process is critical to the

long-term stability of the battery. The classic explanation for dendrite formation is that it occurs during the electroplating process due to limited ion transport in the electrolyte. Based on past research, Rosso and Brissot *et al.* proposed the model of Sand's time, which had a wealth of data on the nucleation and development of Li dendrites over time.[40–42] Sand's time refers to the time when the ion concentration on the electrode surface decreases from the initial concentration to 0 mol L^{-1}. The model could be depicted as shown in the following equation

$$\tau = \pi D\left(\frac{eC_0}{2j}\right)^2\left(1+\frac{\mu_{Li^+}}{\mu_a}\right)^2$$

where τ, J, D, and e are the time when Li dendrites begin to form, effective current density, diffusion constant, and charge, respectively. C_0 refers to initial concentration, which represents Li^+ and anion mobility. The principle could be applied to the growth process of Na dendrites, which directly relates dendrites to Sand's time. When the surface ion concentration is 0 mol L^{-1}, the Na dendrites begin to emerge and the rate of electrode electroplating is completely determined *via* the ion migration rate. It is pointed out that this model is only suitable for high current density. Nevertheless, several studies have shown that the formation of Na dendrites occurs at medium or even low current densities.[40,43,44]

Generally, the sequential growth process is used to explain how Na dendrites grow, which demonstrates how the uneven SEI film is caused by the inhomogeneity of the Na surface. The electroplating of Na^+ on the inhomogeneous Na surface is not uniform, causing ion transport to concentrate in the bumps, and eventually form dendrites.[45,46] The formation of Na dendrites induces the fracture and recombination of SEI films, electrolyte depletion, and safety issues for SMBs. Firstly, the separator is pierced by the Na dendrite formation, which could lead to an internal short circuit of SMBs. Meanwhile, the battery would become extremely hot, which could result in significant safety incidents. Secondly, some Na dendrites are still present. A portion of the dendritic will be discharged into the electrolyte when the stripping position is near the base of the dendrite, producing "dead Na", leading to low CE and capacity decline of SMBs. In addition, "dead Na" may cling to the surface of Na, causing the polarization of the battery to gradually rise and eventually fail.[38] Therefore, Na dendrites formation will affect the cycle stability and safety of SMBs, and it is crucial to induce the uniform Na^+ flux distribution and Na stripping/plating process on the surface of Na anode.

2.3 Volume expansion of Na metal

Na metal dendrites will form during the deposition of Na, which has a significant impact on the cycle stability of SMBs. In addition, the Na metal battery will experience uncontrollable volume change throughout the battery operation owing to the repeated Na deposition/stripping processes.

Compared with the traditional SIBs, the Na^+ storage in the SMBs is largely from the Na metal anode. The metal anode used in the SMBs is a process of electroplating through Na^+ to convert into solid metal deposition. In this process, the size difference between Na atom and Na^+ is an important reason for the volume change of Na anodes.[47,48] The volume change of solid metal is significantly higher than that of traditional graphite intercalation materials. Traditional intercalation materials will provide a specific space to accommodate Na^+, while the electrochemical process of sodium metal electrode takes place on the anode surface. The anode suffers from the pulverization and volume change problems during the cyclic deposition/stripping process, with "dead sodium" scattered in the electrolyte (together with the growth process of Na dendrite). This uncontrollable volume change in the Na anode will eventually increase the over-point position on anode surface, increase the internal resistance, and damage the cycle stability of SMBs.[49]

The original SEI layer faces difficulties due to the volume change of the sodium metal anode. The SEI layer will crack when the mechanical strength of the produced SEI is insufficient. The sodium metal electrode is continuously corroded by the electrolyte from the location where the SEI layer cracks, resulting in the loss of Na metal and electrolyte, which would decrease the CE and cycle life of SMBs.[42] In general, the volume expansion of Na metal anode could be accommodated by 3D conductive frames, which will be discussed in-depth in the coming chapters.

3. Strategies to resolve the issues of Na metal electrode

Therefore, the practical application of Na metal anodes is limited by the above issues of unstable SEI formation, uncontrolled dendrite growth, dramatic volume change, and gas generation during the charging/discharging process. Significant progress has been made in the development of high-performance SMBs to deal with the problems of Na metal anodes during cell cycling. The structural/interfacial engineering on Na metal anode is emerging to regulate Na plating/stripping behavior and improve the cycling stability of SMBs (Fig. 4). A brief description of the common methods is presented to address the Na electrode problems in Table 1, demonstrating the advantages and disadvantages of different strategies in stabilizing the SEI layers on Na metal anodes.

(1) *In situ* SEI construction.[50–52] To promote Na^+ transport and address battery polarization brought by slow ion transport rate, the SEI film can be produced *in situ* on the surface of Na metal electrode using electrolyte additives. In addition, the Na electrode can be effectively protected using the chemical inertness of the *in situ* SEI film, and the low CE initiated by the chemical reactions between the electrolyte and Na metal can be improved. The dendritic growth issue caused by surface inhomogeneity can also be resolved by the production of a uniform SEI layer.

(2) Artificial SEI modification.[53–55] The artificial SEI layer is applied to block the direct contact between the Na metal and

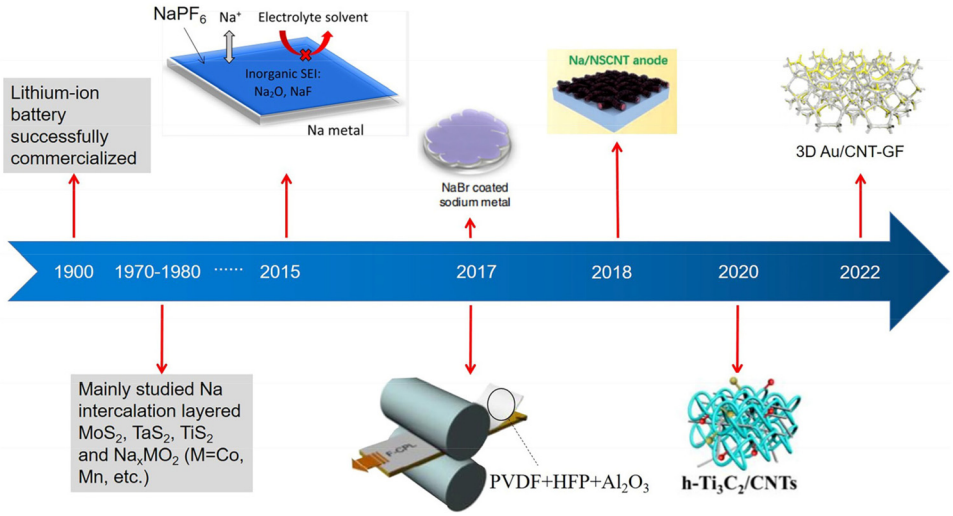

Fig. 4 Development history of interface treatment methods for Na anode.[30,31,60–64] (Reprinted with permission from ref. 60, 61, 30, 31, 62, 63 and 64. Copyright 2015 American Chemical Society, Copyright 2017 The author(s), Copyright 2017 American Chemical Society, Copyright 2018 WILEY-VCH, Copyright 2020 WILEY-VCH, Copyright 2022 Published by Elsevier B.V. and Copyright 2022 The Royal Society of Chemistry).

Table 1 Advantages and disadvantages of different strategies for protecting Na anode

Strategies for Na metal protection	Advantages	Disadvantages
Artificial SEI	1. The SEI layer with high mechanical strength can be constructed 2. Na electrodes can be treated with substances insoluble in conventional electrolytes 3. The SEI layer with complex components can be constructed	The SEI layer ruptures and it cannot be repaired
In situ SEI	1. *In situ* SEI layer can be formed continuously in the presence of electrolyte additive 2. The *in situ* construction is simple for battery operation	1. When the effective substance in the electrolyte is depleted, it cannot be repaired to ensure the integrity of the SEI layer 2. Additives should be soluble in defined electrolytes 3. The composition of the *in situ* SEI layer is the individual component
3D skeleton	1. 3D skeleton can reduce the local current density on the Na anode surface 2. 3D skeleton with a porous structure can accommodate the volume change during Na striping/plating processes	1. 3D skeleton may consume a large amount of electrolyte 2. The 3D skeleton may decrease the whole mass energy density of SMBs

the electrolyte before cell assembly, which is convenient to adjust the mechanical strength and homogeneity of the SEI layer. Through the artificial construction of SEI film, it can effectively promote Na^+ transfer rate and protect the Na metal anode from electrolyte corrosion.

(3) 3D conductive framework.[56–59] The 3D conductive framework can reduce the current density of the electrode, promote the uniform deposition of Na, and reduce the formation of Na dendrite. Moreover, the 3D conductive frame can also accommodate Na metal, reducing the battery failure caused by the volume expansion of Na electrode during the deposition process.

3.1 *In situ* SEI construction

In situ SEI construction is frequently used in the protection of alkali metal anodes as a direct and practical method. The surface of the Na metal electrode can be altered *in situ* by the SEI layer, allowing for a rapid and even deposition of Na metal. The durability of the battery cycling is impacted by the side reaction at the interface between sodium metal and the electrolyte as well as the behavior of Na^+ deposited on the electrodes. The construction of an SEI layer with stable structure and high Na^+ transport rates on the Na interface is the main goal of the current research. It is essential to control the electrolyte components in SMBs to produce SEI layer *in situ*, including the investigation of solvent, sodium salt, and electrolyte additives. The construction of *in situ* SEI layer could be carried out from the following three aspects.

3.1.1 Regulation of solvent structures. Generally, a solvent serves as an essential component of the electrolyte and creates a favorable environment for Na^+ transport in SMBs. As Na^+ is transported by the electrolyte, the ion conductivity of electrolytes has a significant impact on the energy density, cycle life, and safety performance of SMBs.[65–68] The ideal electrolytes

should have the following properties:[69] (1) A wide temperature operating range for battery operation. Within a wide range of temperatures, the melting and boiling points of electrolytes should be markedly below and above the operational temperature, respectively. (2) High ionic conductivity. High ionic conductivity is necessary to ensure the quick passage of Na^+ during battery operation, and the ideal electrolyte should have a reduced dielectric constant and viscosity. (3) Good chemical and electrochemical stability. The voltage range between the oxidation/reduction reaction should within the electrochemical window. According to earlier studies, the energy difference (E_g) between the LUMO and the HOMO in the electrolyte is directly related to the electrochemical window.[35] (4) Ecofriendly. Electrolytes should be free of harmful substances to environment and exhibit sustainability in SMBs. Solvents in electrolytes have recently been the subject of in-depth research, including organic electrolytes (ethers and esters), high concentration electrolytes, and ionic liquids. The drawbacks and benefits of each kind of electrolytes used in SMBs are described in depth below.

3.1.1.1 Ester and ether solvents. In 1990, Dahn *et al.* had extended battery cycle life to thousands of cycles by constructing passivation layers on the surface of graphite electrodes using EC to replace PC as the primary solvent in LIBs.[70] Since then, commercial LIBs have traditionally used the ester electrolyte (1 M $LiPF_6$ in EC mixed solvent with linear carbonates). In general, the most widely used electrolytes are based on molecular solvents such as ester and ether electrolytes.[71,72] Ester solvents are utilized in various electrolytes due to their broad electrochemical windows. However, traditional ester-based electrolytes show potent side reactions with Na anode. Taking PC as an example, Na will undergo a chemical reaction when it comes into contact with PC, creating an unstable SEI layer made up of Na_2CO_3, NaO_2CH, and NaO_2COR. Na metal continuously reacts with the electrolyte due to the unstable SEI layer on Na anode, causing a large amount of electrolyte to be used and lowers the CE of the battery.[37,73] In contrast, the ether-based electrolyte has a greater LUMO energy level than the carbonate ester electrolyte; thus, it is less reactive with Na metal. Salts in the ether-based electrolytes with high LUMO energy level will preferentially react with Na metal, forming a uniform SEI layer with a low surface energy barrier and high Na^+ conductivity. However, the electrochemical windows of ether electrolytes are usually below 4 V, and electrolytes with long-term exposure to voltages higher than 4 V will decompose, which will reduce the cycle efficiency of SMBs.[74]

As ether electrolytes come into touch with a sodium metal surface, they react to form a thick SEI layer with low permeability of Na^+. Therefore, increasing interfacial ion conductivity of the SEI layer is the main subject in ether-based electrolytes. Ether-based electrolytes are widely used in LIBs, while the related studies on fluorine ether in SMBs are scarce.[75–81] Yi *et al.* used an ether-based electrolyte consisting of 1 M $NaPF_6$ in DME, FEC, and 1,1,1,3,3,3-hexafluoroisopropylmethyl ether (HFPM) (2 : 1 : 2, volume ratio) in SMBs.[82] The addition of HFPM contributed to the formation of a stable SEI layer on the Na anode, reducing the vigorous reaction between FEC and Na metal. As a result, the Na||Na symmetric battery with the $NaPF_6$-DME-FEC-HFPM electrolyte exhibited a cycle life of over 850 h and a low polarization voltage of ~70 mV at 1 mA cm^{-2}. In addition, the Na||NVP full cell with the $NaPF_6$-DME-FEC-HFPM electrolyte showed good long-term stability after 2000 cycles and high average CE of 99.9% even at 5 C.

The original SEI layer formed in the ester electrolyte is loose and unstable due to the serious side reaction between abundant polar groups of ester solvent and Na metal. Therefore, the development of a uniform and thick SEI layer on the surface of Na metal anode is encouraged in ester-based electrolytes in SMBs. Significant advancements have been made in the study of lithium metal batteries because LiF is one of the primary elements of the SEI barrier.[83,84] Similarly, NaF could be used to enhance the stability of SEI layers on Na anode by fluoridating the solvents in SMBs.

Solvent, sodium anions, and additives compete for space on the surface of the Na electrode, and the component with the strongest interaction with the electrode surface becomes the primary constituent of the SEI layer. Energy analysis suggests that materials with lower LUMO level will be reduced more frequently at a higher potential. However, the solvation effect in the solution will change the LUMO energy level of the substance. For instance, pure EC molecule has a higher LUMO level than that of the FEC molecule, while the solvation effect of EC with Na^+ will enable EC with a comparable LUMO energy level to FEC in the electrolyte.[39,85] Many researches have shown that the degree of fluorination of solvent will affect its solvation ability in electrolyte. The higher the degree of fluorination of the solvent, the lower the solvation ability in the electrolyte.[86] As a result, the solubility of Na salt in the electrolyte will decrease under a high degree of fluorination of the solvent. Amine *et al.*[87] discovered that FEC molecules cannot form a stable SEI layer on the Na surface until the solvation number is more than one. Therefore, it is important to balance the relationship between solvation ability and the degree of fluorination during the fluorination process of solvents. Lee *et al.* demonstrated a combined electrolyte of 1 M NaFSI and FEC solvent to enhance the reversibility of Na stripping/plating in Na/Cu cells, displaying outstanding cycling performance at 2.82 mA cm^{-2} and comparatively stable voltage response.[88] In contrast, the Na||Cu cell in 1 M NaFSI in EC/PC (1/1) electrolyte with 1 wt% FEC showed a sharp capacity reduction at 0.056 mA cm^{-2}, indicating the rapid consummation of 1 wt% FEC additive.

3.1.1.2 Ionic liquids (ILs). ILs offer low flammability, excellent thermal stability, and low volatility, which can effectively increase the safety and working temperatures of SMBs.[89,90] Besides, ILs have tunable solubility due to the interaction of hydrophobicity, hydrogen bonding, and static electricity in ionic liquids.[91] At the same time, ILs can also withstand the strong reducing and oxidizing reactions from the positive and negative electrodes, respectively.[97–99] Although ionic liquids have several advantages, they have relatively low levels of Na^+ migration and ionic conductivity due to their high viscosity and strong binding to Na^+. IL electrolytes typically have an

order of magnitude lower ionic conductivity than organic liquid electrolytes. In addition, the large polarization and accumulation of anions caused by the coupled diffusion of Na^+ to anions would result in a decline in the cycle life and the electrochemical performance of SMBs. The above defects restrict the further practical application of ILs in SMBs.[91–95]

ILs dissolved with various Na salts could be used as electrolytes in Na-based batteries.[96–98] By altering their structural makeup, ILs can give electrolytes better electrochemical and interface stability. Imidazonium, pyrrolionium, and phosphonium cations are common cations, and $[BF_4]^-$, $[FSI]^-$, and $[PF_6]^-$ are the corresponding anions,[121] which will affect the properties of ILs with different combinations of ions. The bulk viscosity of the ILs rises along with the ionic radius of the cations, which leads to a decrease in the ionic conductivity. Generally, anions with large size do not always cause increased viscosity, while anions with asymmetric structure can affect the viscosity of ILs by altering its melting point.[90]

Typically, many of the anions in ILs are F-containing anionic groups, which contribute to the formation of the SEI layer on the surface of the Na anode. Besides, the F-containing anionic groups could combine with the added sodium salts, increasing the NaF component in the SEI layer.

Makhlooghiazad *et al.* used a tributylmethylphosphonium bis(fluorosulfonyl)imide ($P_{111i4}FSI$) ionic liquid as an electrolyte and added different concentrations of NaTFSI to it for research.[99] An Na||Na symmetric battery was assembled after adding 90% $P_{111i4}FSI$/NaFSI electrolyte. The battery assembled using this electrolyte exhibits a polarization voltage of 10 mV at 90 °C (Fig. 5a). An impedance test was performed on it. The interface resistance after the cycle is significantly lower than the interface resistance before the cycle. This fully demonstrates that the formation of a layer of NaF on the Na metal surface is conducive to the transmission of Na^+ and reduces the interface impedance of the battery. Through the energy dispersive X-ray spectroscopy (EDX), it can be clearly seen that there are a large number of P and F elements on the surface of Na metal, which can effectively protect the Na metal electrode and provide a faster ion transfer rate (Fig. 5b).

In the ILs without fluorine, the effective component of the SEI layer on the surface of Na metal is affected by the solvation effect of cathode additives on the ILs. Forsyth *et al.*[100] added fluorinated anions (PF_6^-, $TFSI^-$, (fluorosulfonyl)(trifluoromethanesulfonyl)imide ($FTFSI^-$), and FSI^-) in a methylpropylpyrrolidinium dicyanamide ([C3mpyr]DCA) IL to regulate the interfacial electrochemistry of the SEI layer on the Na

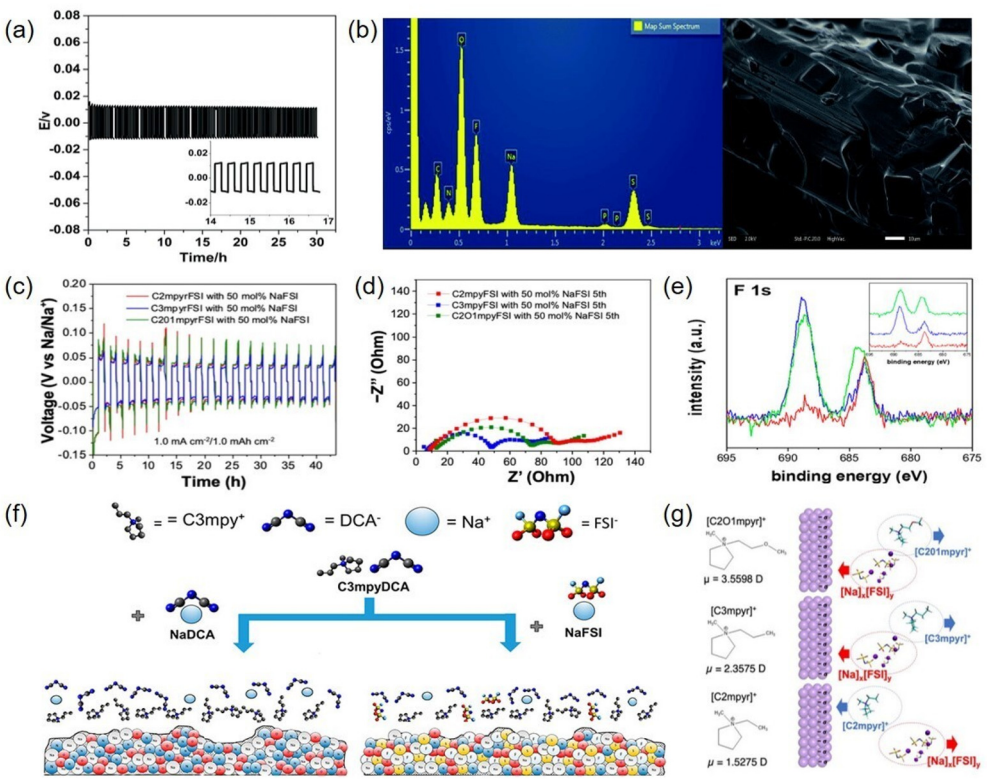

Fig. 5 (a) Galvanostatic curves of 90 mol% $P_{1i444}FSI$/NaFSI at 90 °C at a current density of 0.1 mA cm^{-2} with a cycling period of 10 min. (b) EDX spectrum of 90 mol% NaFSI/$P_{1i444}FSI$, showing high intensity of O, F, and S and low intensity of C and P.[99] (c) Chemical structures of electrolyte components and the corresponding dipole moments of different cationic salts in ILs.[100] (d) F 1s spectra of various anionic ions in ILs.[100] (e) Schematic diagram of different anionic salts in ILs.[101] (f) Nyquist plot recorded for the cells after 5 cycles.[101] (g) The voltage profiles of the Na/Na symmetrical cells at 1.0 mA cm^{-2}/1.0 mA h cm^{-2}. (Reprinted with permission from ref. 99, 100 and 101. Copyright 2017 The Royal Society of Chemistry, Copyright 2022 American Chemical Society and Copyright 2019 American Chemical Society).

anode (Fig. 5c). On the surface of the Na electrode, NaFSI was promoted to form a stable SEI layer with NaF as its primary component (Fig. 5d), while bis(trifluoromethylsulphonyl) imide sodium salt (NaTFSI) and NaFTFSI mostly existed as fluorinated anions on the surface of Na metal.

Cationic regulation is also essential in ILs, and the polarity and redox durability of cations could influence the electrochemical performance of SMBs. Rakov *et al.* regulated the surface structure of Na metal with different polar cations in NaFSI-concentrated IL electrolytes (Fig. 5e).[101] In comparison to the IL cations with more polar and greater dipole moment (μ), such as *N*-methyl-*N*-propylpyrrolionium $[C3mpyr]^+$ and *N*-methyl-*N*-methoxy-methylpyrrolionium $[C2O1mpyr]^+$, the less polar cations with small μ(*N*-methyl-*N*-ethylpyrrolionium $[C2mpyr]^+$) exhibited tighter and more presence on the negatively charged electrode/electrolyte interface. The $[C2mpyr]^+$ with the smallest μ was prone to accumulated copiously on the negatively charged surface of the Na anode, resulting in "blocking effect" with greater energy barrier for Na_xFSI_y during the Na deposition process. In contrast, the impedance experiments revealed that the Na_xFSI_y clusters in highly polar $[C2O1mpyr]^+$ and $[C3mpyr]^+$ systems prior to reduction were favorable for the generation of inorganic rich SEI (Fig. 5f). Moreover, it was found that the electrolyte composed of $[C2mpyr]^+$ showed a higher polarization voltage than $[C2O1mpyr]^+$ and $[C3mpyr]^+$ through the symmetrical battery test, and the $[C3mpyr]^+$ cations with relative reductive stability displayed the most stable SEI layer (Fig. 5g).

3.1.2 Regulation of salt structure and concentration. In addition to the modification of the solvent structure in the electrolyte, it is equally essential to regulate the kinds or concentration of Na salt and additives. These regulation methods could generate different SEI layers on the surface of Na metal anode.

3.1.2.1 Na salt with different types of anions. Apart from the solvent, Na salt, which is frequently employed in electrolytes, is a crucial element in enhancing the cycling performance of SMBs. The features of Na salts that are frequently employed in SMBs are listed below (Table 2). In summary, the compositions of electrolytes are crucial to the long-term stability of SMBs, and the development and exploration of novel electrolytes is particularly crucial in the advanced SMBs system. Even though new electrolyte formulations and different organic electrolytes have been put forward, further study is still required to elaborate the nature of electrolytes and how they interact with electrodes. The optimization of electrolyte formulation has always been an important field for high-performance SMBs. The electrolyte additives commonly used include $NaPF_6$,[102] $NaClO_4$,[88] NaTFSI,[103,104] NaFSI,[128] and NaOTf.[105,106]

Table 2 Typical Na salts and their properties[69]

Name	M_w [g mol^{-1}]	T_m [°C]	σ [mS cm^{-1}]
$NaClO_4$	122.4	468	6.4
$NaBF_4$	109.8	384	—
$NaPF_4$	167.9	300	7.98
NaOTf	172.1	248	—
NaTFSI	303.1	257	6.2
NaFSI	203.3	118	—

The NaF-based *in situ* SEI layer could be constructed by modifying the structure of fluorine-containing Na salts, depositing a NaF-rich SEI layer on the surface of Na metal. Ma and colleagues introduced the 4-acetylpyridine (4-APD) with electron-withdrawing acetyl group to the $NaPF_6$/EC/DEC electrolyte in SMBs. The acetyl group increased more PF_6^- anions coordinated in the Na^+ solvation structure, accelerating the decomposition of PF_6^- to the form a NaF-rich SEI layer. With the 1.0 wt% addition of 4-APD, the Na/Na symmetric battery delivered a long cycling life for over 360 h at 1.0 mA cm^{-1}.[107] Besides, Cui *et al.* proved that NaF can protect the Na anode by adding $NaPF_6$ into the ether-based electrolyte, forming an SEI film composited of Na_2O and NaF on the surface (Fig. 6a).[60] The primary element in organic components was RCH_2Na. When different sodium salts (*e.g.*, NaTFSI, NaFSI, NaOTf, and $NaClO_4$) were added in diglyme, the CE of SMBs decreased obviously upon battery cycling (Fig. 6b).

The existing protection methods of sodium metal have not addressed the effect of the F source in the SEI layer on Na metal, but the difference in the F source in lithium metal batteries is involved in the distribution of LiF and the effect on the cycle performance of Li metal, which is crucial to further studies for the cycle stability of SMBs.[84]

The addition of sodium salt containing F atoms into SMBs is thoroughly explained, which produces an NaF layer on the Na surface to stabilize the Na metal. However, F-containing salts have the tendency to hydrolyze in the presence of trace water and generate a certain amount of HF byproducts during the reaction process, which somewhat constrains their application in electrolytes. Another way to increase the interfacial stability of Na metal is building a F-free SEI layer on the surface of Na metal through the control of sodium salt anions without F.

Kim *et al.*[108] created a "fluorine-free" electrolyte using $NaBH_4$ as an electrolyte additive in diglyme in Fig. 6c, which produced the primary components of $NaBO_2$ and NaH in the SEI layer on the Na surface, according to time-of-flight secondary ion mass spectrometry (TOF-SIMS). Under 1 mA cm^{-2} and 1 mA h cm^{-2} conditions, the assembled Na||Na symmetry battery with $NaBH_4$/diglyme electrolyte showed that the polarization voltage was approximately 75 mV at 100 cycles and 60 mV at 500 cycles. In contrast, the symmetrical battery built by the comparison electrolyte of $NaClO_4$ EC/PC with 5 wt% FEC failed after only 150 cycles (Fig. 6d). Tomich *et al.* tried the Na–Al half battery using fluorine-free $[Na]^+[HCB_{11}H_{11}]^-$ (recorded as Na^+**1**) carbon-aryl electrolyte (Fig. 6e).[109] The average CE of the Na–Al half battery using Na^+**1**/diglyme electrolyte was 98.6%, while the distributed CE for the $NaPF_6$/diglyme electrolyte was 103%. As a result, this test made it clear that Na^+**1** in diglyme solution showed better electrochemical performance than that of $NaPF_6$.

3.1.2.2 Regulation of Na salt concentration. Researchers have created electrolytes with unique purposes in addition to esters

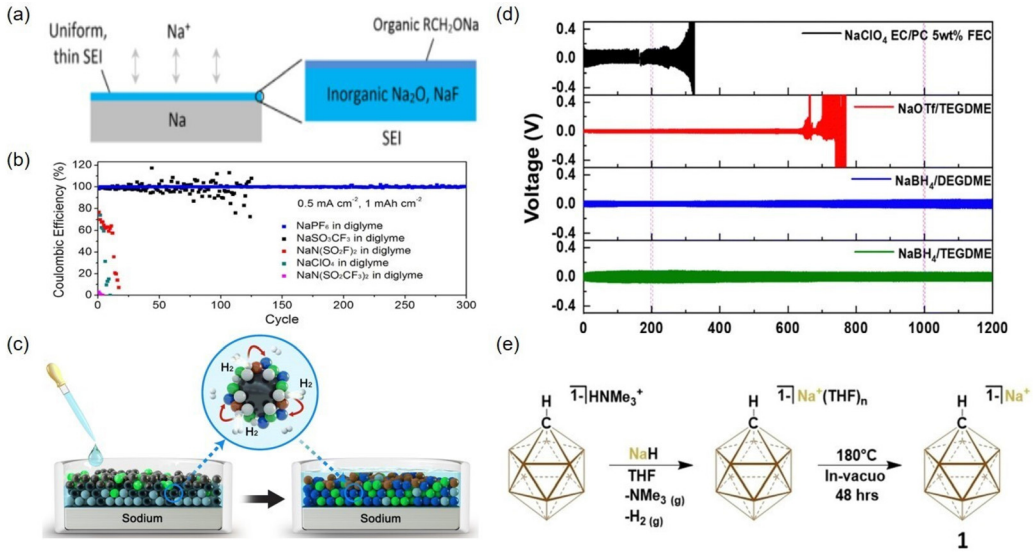

Fig. 6 (a) The schematic diagram of the SEI layer formed on the Na metal surface using $NaPF_6$ in the electrolyte. (b) The CE comparison of SMBs with various electrolyte salts in diglyme.[60] (c) The proposed formation mechanism of SEI layer on Na anode in $NaBH_4$/diglyme electrolyte. (d) The cycle performance of Na||Na symmetric cells in the electrolytes of (black) $NaClO_4$ EC/PC + 5 wt% FEC, (red) NaOTf/TEGDME, (blue) $NaBH_4$/diglyme, and (green) $NaBH_4$/TEGDME.[108] (e) Convenient preparation process of Na**1** by the deprotonation of $[HNMe_3]^+[HCB_{11}H_{11}]^-$ with NaH.[109] (Reprinted with permission from ref. 60, 108 and 109. Copyright 2015 American Chemical Society, Copyright 2022 Royal Society of Chemistry and Copyright 2022 Wiley-VCH GmbH).

and ethers, which are frequently used as electrolyte solvents. Ionic liquids and high concentration electrolytes have both been examined in addition to the conventional ester and ether electrolytes used in SMBs. High concentration batteries provide steady high voltage performance and a sizable suppression of Na dendrites. For the first time, McKinnon and Dahn proposed a liquid electrolyte system with a high concentration of concentrated electrolyte, which has attracted the attention of numerous research organizations.[110–120] The electrolyte used in SMBs has a significant advance as a result of the work of high concentration electrolyte in LMBs.[121–134] The solvated structure of the high concentration electrolyte is largely responsible for its remarkable chemical characteristics. The location of the LUMO is transferred from the solvent to the salt *via* the new solvation structure. In addition, the less electrode corrosion results from the decrease in the free solvents. However, when the concentration of the salt increases, the viscosity and expense of the electrolytes rise, which will affect the ionic conductivity and wettability of the high concentration electrolyte. One of the most efficient ways to deal with high concentration electrolyte is to add "inert" solvent, which will cause the high concentration electrolyte to transform into local high concentration electrolyte. These inert solvents can reduce its viscosity, improve ion conductivity, and enhance wettability with electrodes without altering the solvation structure in the high concentration electrolyte.[135,136]

In addition to the modification of the SEI layer with different kinds of Na salt on the surface of Na metal, the electrode can be protected by changing the concentration of Na salt. By adding a large amount of sodium salts into the electrolytes, the high concentration electrolytes are achieved to produce a positive effect on the SMBs. High concentration electrolytes have two benefits on the solid–liquid interphase: (1) it can remove unbound solvent molecules from the Na surface, preventing Na metal corrosion and the formation of an unstable SEI layer. (2) There is a significant amount of enriched Na^+ on the Na surface, which can both effectively decrease the Na dendrite growth on the Na surface as well as the battery polarization generated by the concentration difference. Chen *et al.* elaborated that $Na_x(FSI)_y$ was concentrated on the anode surface to separate the organic solvent from the Na anode.[135] By efficiently preventing the production of the unstable SEI film, this high concentration electrolyte might shield the Na anode from organic electrolyte corrosion. In addition, surface-attached FSI^- could interact with Na to create NaF-based SEI layer, which promotes the buildup of Na^+ and prevents Na dendrite growth. However, the Na^+ transmission rate in the high concentration electrolytes decreased obviously due to their high viscosity. To cope with this problem, bis(2,2,2-trifluoroethyl)ether (BTFE) was added to form a locally-concentrated electrolyte (labelled as NaFSI/1,2-dimethoxyethane (DME)-BTFE). The CE of the assembled Na–Cu half-cells with different electrolytes was tested at 1 mA cm^{-2} and 1 mA h cm^{-2}. The 5.2 M NaFSI/DME electrolyte was used to obtain an average CE of 98.5%, while the locally concentrated electrolyte of 2.1 M NaFSI/DME-BTFE (1 : 2) displayed an average CE of 98.95% after over 400 cycles. In Na||NVP, the 1.7 M NaFSI/DME electrolyte quickly failed. With a capacity retention rate of 90.8%, the 2.1 M NaFSI/DME-BTFE (1 : 2) electrolyte could deliver a capacity of 66.4 mA h g^{-1} at 20 C after

40 000 cycles. In contrast, the Na||NVP cell with 5.2 M NaFSI/DME electrolyte exhibited a capacity of 24.0 mA h g^{-1} and a capacity preservation rate of 48%. Besides, many researches focused on solving the problem of low bulk-phase ionic conductivity of high concentration electrolyte,[133–135] and the details would not be depicted in this topic.

3.1.3 Additive. The modification of anions is mainly focused on Na salt regulation. One of the compounds is for adding organic material with functional groups, and the other is for adding cationic salts other than Na^+. The various kinds of additives are described in depth below.

3.1.3.1 Organic additive. The two basic ways that organic electrolyte additions can boost battery performance are: (1) Enhance the properties of electrolytes, for example, by improving its heat stability or expanding its electrochemical stability window. (2) Through the reaction with the Na anode to produce an *in situ* SEI film on the electrode surface. This SEI layer can effectively isolate the electrolyte corrosion to Na anode, promoting the deposition of Na^+ on the anode surface. The SEI film (including elements such as F, Br, and P) is primarily formed on the Na anode surface. Li *et al.* introduced cetyltrimethylammonium bromide (CTAB) as an electrolyte additive into $NaPF_6$-diglyme electrolytes (Fig. 7a).[137] On the Na anode, the CTAB molecule resolved into the ions CTA^+ and Br^- to form a SEI layer with NaF and NaBr species, which guaranteed that Na^+ was evenly distributed on the surface of Na metal (Fig. 7b). With the addition of 5 mM CTAB electrolyte, the symmetrical battery could cycle for 400 h after failing on the ninth cycle at 10 mA cm^{-2}. The Na–S full battery with electrolyte containing 5 mM CTAB demonstrated a capacity of 640 mA h g^{-1} and a CE of 98.7% CE at 0.5 C, outperforming the battery using a neutral electrolyte.

Organic electrolytes with FEC might create an SEI layer containing NaF on Na metal. Besides, FEC could be employed as an electrolyte potentially that retards flames. Luo *et al.* designed a safe SMBs based on 1.0 M $NaPF_6$ electrolyte in FEC/PC/1,1,2,2,2-tetrafluoroethylene-2,2,3,3-tetrafluoropropylene ether (HFE) and perfluoro-2-methyl-3-pentanone (PFMP).[138] In this electrolyte formulation, FEC acted as a "bridging solvent" to promote the mutual dissolution of the two liquids (Fig. 7c). In addition, FEC could produce NaF on the surface of Na metal to shield the Na anode from electrolyte corrosion and extend the battery life. It was clear from the precise voltage distribution that the conventional 1.0 M $NaPF_6$ in ethylene carbonate (EC)/PC (1 : 1 vol%) (referred to as N-EP) electrolyte was experiencing significant voltage variations and an increasing overpotential (the 50th cycle was 760 mV). While utilizing 1.0 M $NaPF_6$ in FEC/PC/HFE (referred to as N-FEPH) and N-FEPH + PFMP electrolytes, the plating/stripping polarization of batteries was restricted to 160 and 90 mV (Fig. 7d). Vinyl carbonate, trimethylsilane phosphite, Na difluoro(oxalic acid)borate, and other substances could be employed as organic electrolyte additives as well. The initial capacity of the $Na/Na_3V_2(PO_4)_2O_2F$ full cell evaluated at 0.5 C was 120 mA h g^{-1}, and the CE was 94.7% with the N-FEPH + P electrolyte, compared to 89.1% with the N-EP electrolyte.

Jiang *et al.* suggested a method to create ULCE + 2 wt% BSTF by adding *N,O*-bis(trimethylsilyl) trifluoroacetamide (BSTF) as an adjuvant to 0.3 M $NaPF_6$ + EC/PC (1 : 1 vol%) extremely low concentration electrolyte (ULCE) as the neutral electrolyte (blank).[139] The introduction of BSTF served as an ionic carrier NaF, which possibly contributed to the removal of HF and H_2O from the electrolyte and the inhibition of $NaPF_6$ hydrolysis. In an impedance measurement, the interface impe-

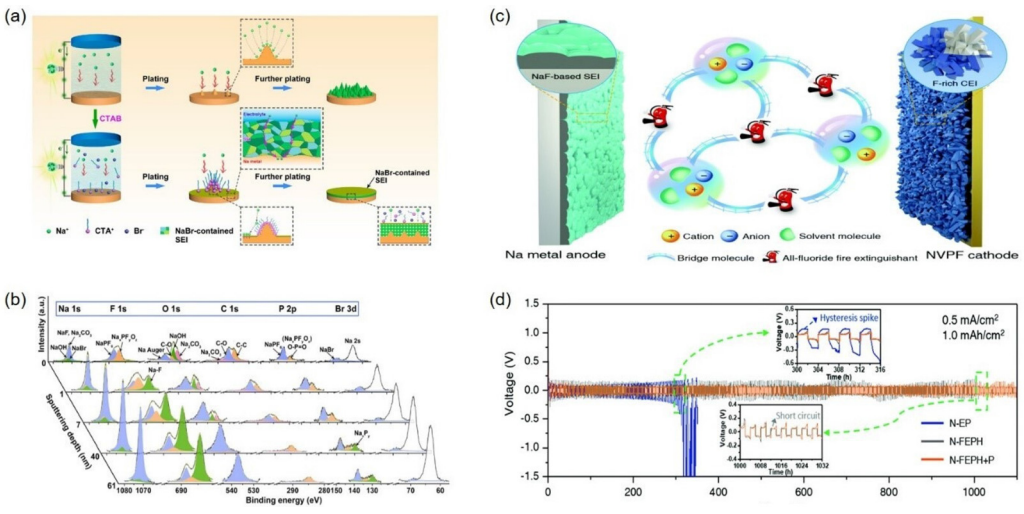

Fig. 7 (a) Diagrammatic representation of the effect of CTAB electrolyte additive on the Na deposition procedure. (b) X-ray photoelectron spectroscopy depth profile analysis of the SEI layer produced in an electrolyte comprising CTAB and $NaPF_6$-diethylene glycol.[137] (c) Schematic diagram of the SMB with an all-fluoride electrolyte by the connection of a bridge molecule. (d) Comparison of constant current plating/stripping process of Na in Na/Na symmetric cells at 1.0 mA cm^{-2} and 1.0 mA h cm^{-2}.[138] (Reprinted with permission from ref. 137 and 138. Copyright 2022 American Chemical Society and Copyright 2020 The Royal Society of Chemistry).

dance of ULCE + 2 wt% BSTF-modified electrolyte was 85.2 after 20 cycles on the Na electrode surface, which was lower than that of ULCE (461.4). The entire Na||NVP battery with ULCE + 2 wt% BSTF demonstrated the average CE of 92.63%, while the ULCE/blank-based cells (with 1 M $NaPF_6$ EC/PC (1 : 1 vol%)) failed after 650 and 800 cycles, respectively. These results demonstrated that the BSTF additive can effectively promote the application of a low concentration electrolyte.

Moreover, the production of a functional organic polymer on the surface of Na metal can result in an *in situ* SEI layer as well. Wei *et al.* generated a ionic polymer film on the surface of Na anode through the electropolymerization of an imidazole cationic ionic liquid monomer (Fig. 8a).[140] The surface impedance in the symmetrical battery using electrolyte without 1,3-diallyl imidazolium perchlorate (DAIM) grew unsteadily. By contrast, it was discovered that the impedance of the symmetrical battery increased consistently after 2 h of circulation with a 20 wt% DAIM electrolyte, demonstrating that an SEI layer developed over time on the electrode surface (Fig. 8b). The electrode impedance remained consistent, following a stable increase when DAIM was added into the battery, indicating that a stable SEI film had developed on the surface (Fig. 8c). As a result, the full battery showed a CE of 96% and a capacity of 97 mA h g^{-1} after 160 cycles (Fig. 8d).

3.1.3.2 Inorganic additive. Organic electrolyte additives have their own functional groups that can protect Na metal surfaces. The inorganic electrolyte additive can produce a stable and uniform SEI layer on the surface of Na metal *via* chemical interaction with Na metal.

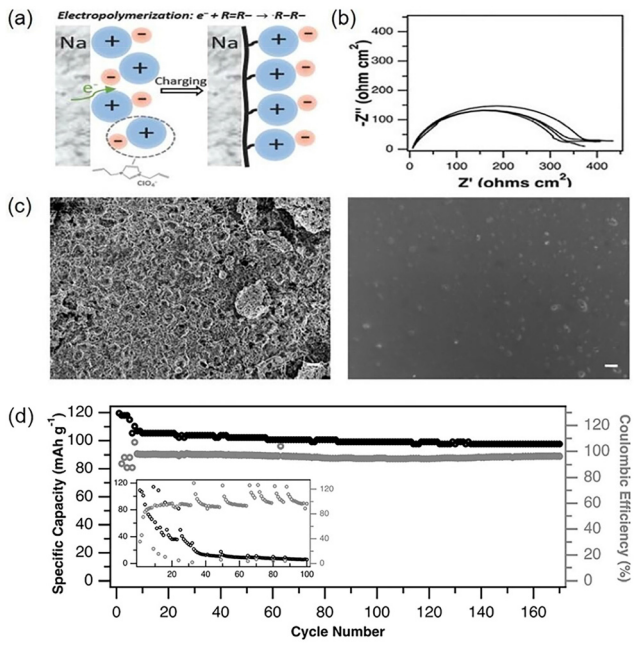

Fig. 8 (a) Diagrammatic representation of the electropolymerization process of imidazole IL on Na metal surface. (b) Nyquist plots of Na||Na symmetric cell following every 2 h charging with DAIM at 1 mA cm^{-2}. (c) SEM images of the Na surface in the symmetric coin cells with and without the addition of DAIM in the electrolytes after 10 rounds of stripping and plating (scale bar: 20 μm). (d) The cycle performance of the full battery with imidazole IL added into the electrolyte.[140] (Reprinted with permission from ref. 140, Copyright 2017 WILEY-VCH).

Carrier ion diffusion in the alloy anode typically results in compressive stress in front of the propagation contact, which prevents carrier ion diffusion and restricts the amount of carrier ions that can fully penetrate the alloy anode during the battery cycle. Self-limited diffusion (SLD) is a phenomenon that restricts the full usage of the anode materials and lowers the rate performance of the battery. Byeon *et al.* showed that the diffusion of Na into Sn crystal would cause tensile stress near the interface and promote the formation of high-density dislocations.[141] By creating a pathway for dislocation tube diffusion and relieving the SLD effect, the ensuing dislocations facilitated the diffusion of Na^+ at an ultrafast rate. Sn or Na–Sn alloy production can efficiently promote the deposition of Na^+ and minimize dendrite formation on the Na surface. Huang *et al.* modified 1.0 M $NaClO_4$ in EC/PC electrolytes using $SnCl_2$ as an electrolyte additive (Fig. 9a and b).[142] The surface of Na would react with the changed electrolyte to generate a Na–Sn alloy and a NaCl mixed SEI layer, protecting Na from reacting with the electrolyte by further passivating the Na surface. The symmetrical battery could cycle steadily for more than 500 h at an overpotential less than 50 mV after adding 50 mM $SnCl_2$ into the carbonate electrolyte. The polarization of the blank battery steadily increased to exceed 100 mV after about 200 cycles. The full Na||NVP battery with 50 mM $SnCl_2$ additive showed a capacity of 87% at 1 C, while the blank one only retained 75% of its capacity. Xiang *et al.* added SbF_3 into the electrolyte to generate NaSb and NaF layers on the surface of Na. The main component of the electrolyte was 2 M NaFSI/DME with 1,1,2,2-tetrafluoroethyl-2,2,3,3-tetrafluoropropyl ether (FEPE) and 1 wt% SbF_3.[143] The assembled full battery (with NVP as cathode) with SnF_3 showed a capacity of 107 mA h g^{-1} at 1 C. The SEI film created after SnF_3 modification could successfully promote the Na^+ transmission rate and the capacity of the sodium metal battery at high magnification.

The use of a salt composed of nonreducible ions (*e.g.*, Li^+ and K^+) as a cationic additive is also a solution, which has functions including electrostatic shielding, optimization of electrolyte solvation structure, and electrolyte stabilization. Chen *et al.* used lithium difluorobis(oxalato)phosphate (LiDFBOP) as an additive in 1 M $NaPF_6$ FEC/DEC (v : v = 1 : 1, labeled F/D(1/1)) electrolyte in SMBs (Fig. 9d).[144] $DFBOP^-$ anions induced a stable film through redox reaction with Na metal, and Li^+ cations could the dendrite-free Na plating *via* electrostatic shielding, both promoting the stability of electrode/electrolyte interphases. Testing revealed that the symmetric batteries with treated electrolyte could maintain a steady cycle for 2600 h while maintaining polarization below 0.25 V (Fig. 9e) (surface capacity of 1 mA h cm^{-2}, current density of 1 mA cm^{-2}), but symmetric batteries without LiDFBOP failed after 880 h. In comparison to F/D (1/1) and EC/PC (1/1) electrolytes, the F/D (1/1) electrolyte with LiDFBOP demonstrated outstanding electrochemical performance (500 cycles of stabilization) in Na||NVPF throughout the entire battery test at 1 C (Fig. 9f).

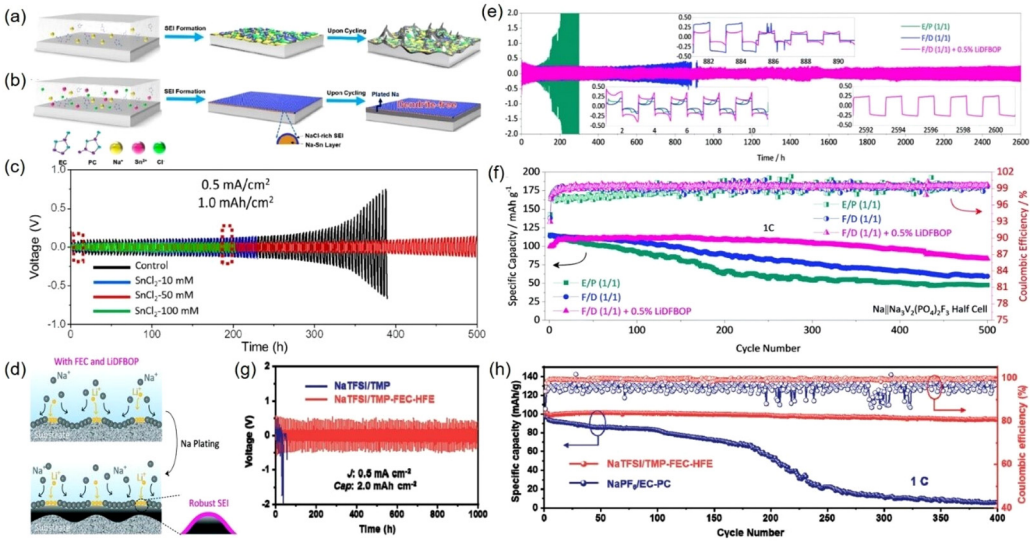

Fig. 9 The schematic diagram of (a) mosaic SEI and (b) dendrite-free morphology of the NaSn alloy layer on Na metal anodes. (c) Cycling stability of Na/Na symmetric cells with different $SnCl_2$ amounts.[142] (d) Schematic diagram of the Na plating process in the FEC and LiDFBOP electrolyte. (e) The cycle performance of Na||Na battery in E/P (1/1), F/D (1/1), and F/D (1/1) with 0.5% LiDFBOP electrolyte formula at a current density of 1 mA cm^{-2} and a capacity of 1 mA h cm^{-2}.[144] (f) The cycle performance of Na||$Na_3V_2(PO_4)_2F_3$ cells in different electrolytes. (g) The galvanostatic plating and stripping behavior of Na/Na symmetrical cells at 5 mA cm^{-2} and 2.0 mA h cm^{-2} in the NaTFSI/TMP and NaTFSI/TMP-FEC-HFE electrolytes. (h) Cycling stability of Na||NVP full cells in $NaPF_6$/EC-PC and NaTFSI/TMP-FEC-HFE electrolytes.[149] (Reprinted with permission from ref. 142, 144 and 149. Copyright 2019 American Chemical Society and Copyright 2022 Royal Society of Chemistry).

SMBs can also receive the addition of K^+ to stabilize the SEI layer on the Na anode. Ji *et al.* added KFSI into the 1 M $NaPF_6$-EC/PC (NaPF-K) electrolyte to improve the cycling stability of SMBs.[145] K^+ served as an electron shield ion in the electrolyte to bind on the surface of Na metal. In addition, the P–F bond in PF_6^- was more readily broken than the S–F bond in FSI^-, which caused a NaF/KF-rich SEI layer on the surface of Na metal. Following the battery test, the NaPF-K assembled symmetrical battery was able to run steadily for 400 h at a current density of 0.5 mA cm^{-2}, and the polarization voltage increased from 260 to 305 mV. Therefore, the integrity of the Na anode during deposition and stripping could undoubtedly be ensured by the NaPF-K electrolyte.

Fullerene (C_{60}) was discovered to have the ability to enhance the surface of Na metal, induce Na^+ deposition after enrichment, and inhibit the growth of sodium dendrites, improving the long cycle life of SMBs. Li *et al.* bound $-NO_2$ to the surface of C_{60} to create the $C_{60}(NO_2)_6$ group, which was introduced as an additive to 1 M $NaPF_6$/DME electrolyte at a concentration of 0.5 mM.[146] The Na||Na symmetric battery with $C_{60}(NO_2)_6$ electrolyte exhibited more than 500 cycles (1000 h) at 2.0 mA cm^{-2} and a low polarization voltage of less than 30 mV, while the unmodified blank electrolyte failed within 100 cycles. Moreover, the assembled Na||Cu battery with 1 M $NaPF_6$/DME and $C_{60}(NO_2)_6$ still maintained high CE even under the condition of 5 mA cm^{-2} and 5 mA h cm^{-2}. Moreover, Li *et al.* formed $C_{60}(CF_3)_6$ by combining C_{60} with the $-CF_3$ group and adding it to 1 M $NaPF_6$/DME electrolyte.[147] The Na electrode surface was able to maintain stable Na^+ transmission and reduce the polarization under the protection of C_{60} and the NaF-rich SEI layer. The symmetric battery in the electrolyte of $C_{60}(CF_3)_6$ and 1 M $NaPF_6$/DME demonstrated a cycle life for over 300 h and a polarization voltage of 30 mV at 5 mA cm^{-2} and 2 mA h cm^{-2}, which was superior to the blank electrolyte. With an initial capacity of 108 mA h g^{-1} in Na||NVP@C full battery with $C_{60}(CF_3)_6$ and 1 M $NaPF_6$/DME electrolyte, 99% capacity retention could be achieved after 1000 cycles at 1.5 mA cm^{-2} but only 65% with 1 M $NaPF_6$/DME under the same condition. It was evident that C_{60}-based salts are promising in the electrolyte modification of SMBs.

3.1.4 Coupling additives and high concentration salt for the *in situ* SEI layer. Electrolyte additives can play a role in high concentration electrolyte. The arrangement of free solvent molecules in the high concentration electrolyte is altered by the abundance of solute molecules. In combination with electrolyte additives, the Na anode can be safeguarded and the side reactions in the battery can be decreased by lowering the amount of free solvent molecules on its surface in the high concentration electrolyte. Lee *et al.* added 5 M NaFSI into DME electrolyte to form a high concentration electrolyte in SMBs.[148] The Na/stainless steel cells with the high concentrated electrolyte (5 M NaFSI/DME) had a high CE of 99.3%, while it showed a significant drop in CE at the third cycle with the 1 M $NaPF_6$/EC/PC electrolyte. In addition, the Na||$Na_4Fe_3(PO_4)_2(P_2O_7)$ cell displayed an initial capacity of 109.4 mA h g^{-1} and a CE of 99% at 0.5 C in the 5 M NaFSI/DME electrolyte.

Liu *et al.* introduced 1,1,2,2-tetra-fluoroethyl 2,2,3,3-tetra-fluoropropyl ether (HFE) and FEC into 1 M NaTFSI trimethyl

phosphate (TMP)-based electrolyte, which was assembled into a new high concentration electrolyte (1 M NaTFSI + HFE + FEC + TMP).[149] With a high concentration solution, the symmetric cell made up of 1 M NaTFSI + HFE + FEC + TMP electrolyte maintained a polarization voltage of 120 mV after 1000 cycles at 0.5 mA cm^{-2} (Fig. 9h). Besides, the full Na||NVP battery with 1 M NaTFSI + HFE + FEC + TMP electrolyte showed a starting capacity of 100 mA h g^{-1} and a capacity retention of 93.1% after 400 cycles (Fig. 9g). In contrast, only one experiment could be conducted in the Na||NVP battery with the 1 M NaTFSI + TMP electrolyte. As a result, adding HFE and FEC could not only form a stable SEI on the surface of Na metal but also lessen the amount of free solvent molecules. According to the aforementioned results, sodium salts and other electrolyte additives are crucial for achieving long cycle and low polarization of SMBs, and the *in situ* SEI construction is a practical strategy to achieve high-CE SMBs. The recent reported artificial SEI and related approaches for protecting Na anodes are shown in Table 3.

3.2 Construction of the artificial SEI layer

The cycle stability of SMBs can be successfully enhanced by an *in situ* SEI layer, but the formation of the SEI layer mainly occurs after the battery operation. The pretreatment of Na metal anode to form a stable artificial SEI helps to improve the structural stability of Na metal surface in SMBs. The types of artificial SEI layers can be divided into the following aspects: carbon-based materials, metal oxide materials, alloy materials, and Na salt materials.

3.2.1 Carbon-based material. An uneven SEI coating will result in an unequal electric field strength on the Na surface. Finally, it will result in unequal Na^+ diffusion, which will stimulate the formation of Na dendrites. Carbon materials with flexibility and mechanical strength have drawn great attention since they are common in nature and may be designed to get the desired structure. By altering carbon materials, it is possible to increase the conductivity of Na^+ and electrons. Wang *et al.* used a new protection strategy to treat the collector surface to promote Na^+ deposition under the graphene layer (Fig. 10a).[150] The electrolyte and freshly produced metal could be separated using this "overpotential-induced Na filtration deposition" method. Na^+ was able to pass through the graphene and deposit on the Cu surface because this layer of graphene had a higher overpotential than the Cu collector. A 3D Cu foam surface with this deposited graphene layer (record as NCS-SG) had displayed granular and dendrite-free Na plating/stripping behaviors. The Na–Cu half-cell with the NCS-SG electrode showed a CE of 93.3% after 150 cycles. In contrast, the battery with a flat 2D Cu showed only 84.9% CE after 20 cycles before its failure.

In addition, carbon-based materials with flaws or doped heteroatom structure is better suited to enhance Na^+ transport and further foster Na^+ deposition. Wang *et al.* used N and S-treated carbon nanotubes (NSCNTs) as the interlayer to control the nucleation behavior of Na and inhibit the formation of Na dendrites (Fig. 10b).[31] The sodium affinity of functional groups containing N and S elements on carbon nanotubes could induce the uniform distribution of Na on the NSCNTs layer. The SEM images revealed that the treated anode surface was flattened after 20 cycles (Fig. 10e). The initial polarization voltage of the Na/NSCNT||Na/NSCNT battery was about 70 mV, and the stable cycle could maintain 500 h at 1 mA cm^{-2}. However, the unmodified Na||Na battery showed a lower initial polarization voltage (20 mV) but a short-circuit at 30 h.

3.2.2 Metallic material. Another potential method to stabilize the Na metal and facilitate Na^+ transport is using metallic materials in the modification of SEI layers, such as alloys and metal oxides on the surface of Na metals. Using this design, the electronic conductivity of the metal top layer can be decreased while its Na^+ conductivity and chemical inertness could be improved.

3.2.2.1 Metal oxide. Metal oxides with good Na^+ conductivity are potential candidates for the SEI layer on Na metal anodes to protect Na from corrosive environments. The atomic layer deposition (ALD) technology could control the thickness of the SEI film by the deposition time, investigating the influence of film thickness on Na anode protection and Na^+ trans-

Table 3 The comparison of electrochemical performance of Na metal electrode protected by the *in situ* SEI layer

Na@SEI	Electrolyte	Current density (mA cm^{-2})	Energy density (mA h cm^{-2})	Na/Na cell (cycle life@ overpotential (mV))	Ref.
Na@NaF	1 M $NaPF_6$ in DME + FEC + HFPM (2 : 1 : 2, in volume ratio)	1	1	800 h@52	82
Na@NaF	1 M $NaPF_6$ + [C3mpyr]DCA	0.1	0.1	50 h@10	100
Na@NaH + $NaBO_2$	$NaBH_4$ + diglyme	1	1	1200 h@50	108
Na@Na_2CO_3 + Na_2O	Na^+**1** + DME	2	1	300 h@30	109
Na@NaF	2.1 M NaFSI/DME-BTFE (1 : 2)	1	1	1000 h@>60	135
Na@NaF + NaBr + CTA^+	5 mM CTAB + $NaPF_6$-diglyme	10	30	400 h@—	137
Na@NaF	1.0 M $NaPF_6$ + FEC + PC + HFE + PFMP	0.5	1	4400 h@90	138
Na@NaF	0.3 M $NaPF_6$ + EC/PC (1 : 1 vol%) + 2 wt% BCTF	0.5	0.5	350 h@153	139
Na@DAIM	20 wt% DAIM + carbonate-based electrolyte	1	1	242 h@55	140
Na@Na-Sn + NaCl	50 mM $SnCl_2$ + 1 M $NaClO_4$ + EC/PC	0.5	1	500 h@100	142
Na@NaF + NaSb	1 wt% SbF_3 + 2 M NaFSI + DME + FEPE	0.5	0.5	1200 h@950	143
Na@Li^- + NaF	LiDFBOP + 1 M $NaPF_6$ in FEC/DEC	1	1	2000 h@150	144

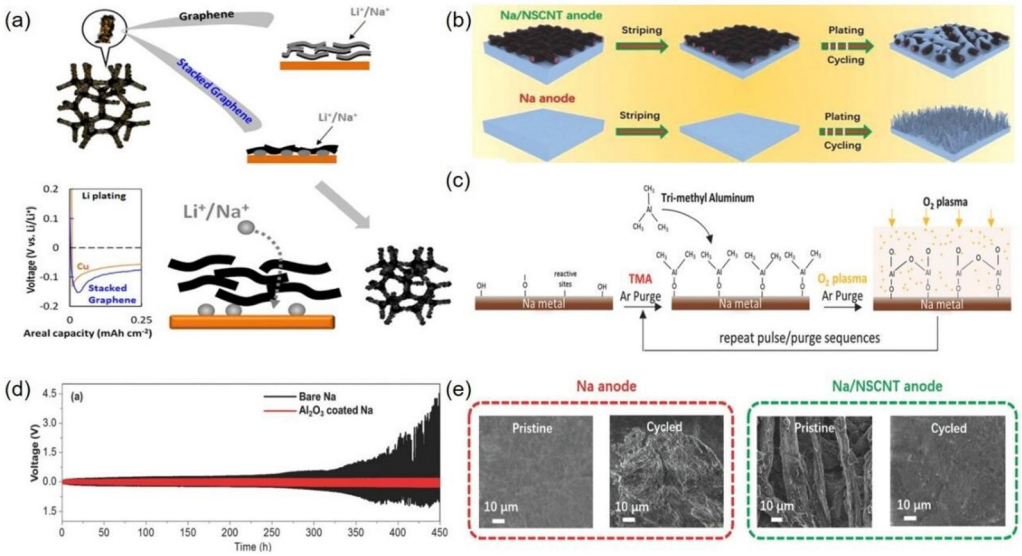

Fig. 10 (a) Schematic diagram of the Li^+/Na^+ deposition process on stacked graphene on copper foam and comparison with the deposition overpotential of bare copper for Li^+.[150] (b) Schematic illustration of Na deposition behavior on the Na/NSCNT and bare Na electrodes.[31] (c) Flow chart of Al_2O_3 thin film preparation on Na surface using ALD technology. (d) The stripping/plating curves of symmetrical batteries with bare Na electrode and the electrode after ALD treatment.[152] (e) SEM images before and after Na deposition on NSCNT-modified and unmodified Na electrodes. (Reprinted with permission from ref. 150, 31 and 152. Copyright 2018 WILEY-VCH, Copyright 2018 Published by Elsevier B.V. and Copyright 2016 WILEY-VCH).

mission rate. Sun *et al.* proved for the first time that ultrathin Al_2O_3 layer prepared *via* ALD technology could effectively protect Na metal.[151] This Al_2O_3 film had the potential to minimize the formation of Na dendrites while also increasing the cycle life of SMBs. Moreover, Luo's research team reported that the low temperature ion-enhanced atomic layer deposition (PEALD) technology was used to cover the Na surface with an artificial SEI film (Fig. 10c).[152] The PEALD technique was used to coat a layer of Al_2O_3 film on the Na surface, which effectively coped with the situation of the experimental temperature being higher than the melting point of Na. The treated Na anode could cycle for 450 h in a low voltage range owing to the isolation effect of the Al_2O_3 film between Na and the carbonate electrolyte. In sharp contrast, the polarization voltage of bare Na anode increased gradually, which eventually led to battery failure (Fig. 10d). Moreover, the treated Na anode had a smooth surface after cycling for 450 h, but the untreated original anode showed dendrites, demonstrating that Al_2O_3 was involved in Na anode protection.

3.2.2.2 Alloy material. Na metal with a highly reactive nature could react with the respective metal to produce the corresponding Na alloy and Na salt. The interface stability of the Na anode can be successfully improved by the composite SEI layer created on the surface of Na metal.

The Na anode could reduce Sn^{4+} to produce the Na–Sn alloy and corresponding Na salts when touched with the solid or electrolyte of Sn salt. Kumar *et al.* reported a method of treating Na anode using gas–solid two-phase. The reaction between $SnCl_4$ vapor and Na metal produced a surface layer containing Na_xSn_y and NaCl (Fig. 11a).[153] This two-material surface layer could effectively shield the Na from electrolyte degradation

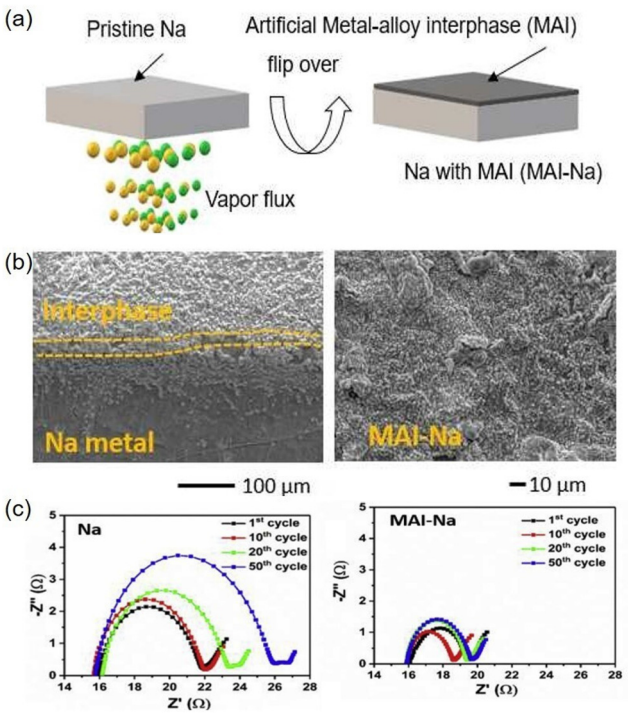

Fig. 11 (a) Graphical representation of the formation process of the artificial MAI on the Na metal interface. (b) Cross-sectional view of bare Na and MAI-Na interface. (c) The EIS of Na//Na cells without and with MAI after different stripping/plating cycles.[153] (Reprinted with permission from ref. 153. Copyright 2020 Elsevier B.V.).

and guarantee the Na^+ transfer rate throughout the Na deposition process. The reaction equation is shown as follows.

$$4Na + SnCl_4 \rightarrow Sn + 4NaCl,$$

$$xNa + ySn \rightarrow Na_xSn_y.$$

Field emission scanning electron microscopy (FESEM) was used to describe the artificial metal alloy interphase (MAI), and the thickness of the MAI was approximately 6 μm (Fig. 11b). The particles were uniformly distributed across the surface of Na, and Na^+ nearly diffused along the *x*-axis in this arrangement. The Nyquist curve revealed that the resistance of the MAI was about 3.5 Ω after the first cycle, while the resistance of the original Na anode was substantially greater. The resistance reduced further after 10 cycles, indicating the low Na^+ diffusion barrier of MAI (Fig. 11c). The MAI-Na||MAI-Na cell showed stable cycles of over 650 cycles at a current density of 2 mA cm^{-2}, while the untreated electrode showed a cycle life of less than 100 cycles. The comparison of the Na–S full cell (0.5 C) showed that the Na||S cell died after 50 cycles, but the average CE of the MAI-Na||S cell remained at 99.7%.

Na–Bi alloy as a protective layer can effectively prevent electrolyte corrosion of the Na anode and can provide excellent ionic conductivity. Sun *et al.* reported that Na powder and Bi powder were mechanically mixed and then compressed to prepare the mixed electrode (Fig. 12b).[154] The mixed electrode could experience a spontaneous alloying event to increase metal surface tension and Na^+ affinity, which could well alter the Na deposition and effectively limit dendrite formation. The symmetrical battery with mixed anode exhibited a overpotential of 20 mV after cycling for 1200 h in carbonate electrolyte, while the original Na electrode failed within 100 h with a polarization voltage of 120 mV. In a flame-retardant electrolyte, the electrode was employed. The full battery with $Na_3V_2(PO_4)_3$ cathode and treated Na showed a CE of 99.9% at 585 mA g^{-1} in a flame-retardant phosphate electrolyte. The Na–Bi alloy combined with Na salt could obtain a high-performance SEI layer as well. Yu *et al.* reacted Na with BiOCl to produce a mixed SEI layer containing Na_3OCl and Na–Bi alloy (Fig. 12c).[155] This SEI served two primary purposes: (1) promotes Na^+ deposition and obtains consistent Na/artificial interface deposition. (2) Prevents the formation of Na dendrites. The SEI layer with Na_3OCl possessed a high Young's modulus and interface energy. The symmetrical battery with treated Na anode demonstrated a low polarization voltage of 30 mV and a steady cycle of 700 h (in carbonate electrolyte) at 1 mA cm^{-2} (Fig. 12d). NVP||Na_3OCl/Na_3Bi@Na batteries showed excellent cycling performance at 15 C (1C = 110 mA g^{-1}) and a reversible capacity of 83 mA h g^{-1} with a CE of ~99.5% after 1500 cycles. In contrast, NVP||Na batteries exhibited rapid capacity attenuation, especially after 500 cycles, which could be attributed to the slow kinetics of the Na anode/electrolyte interface and "dead sodium" production. Chen *et al.* dropped 40 μL 10 mmol L^{-1} of $Bi(SO_3CF_3)_3$ dimethylether electrolyte on the Na surface for the *in situ* reac-

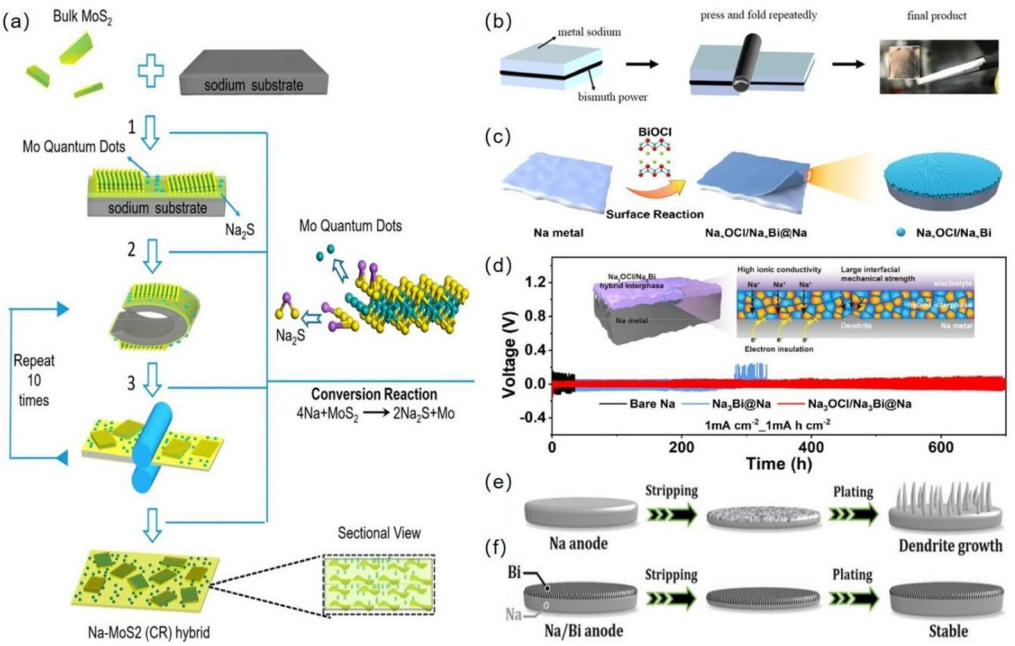

Fig. 12 (a) Manufacturing diagram of the Na-MoS_2 (CR) hybrid. It consists of three steps: (1) dispersing massive MoS_2 onto the surface of a piece of fresh Na, (2) folding the MoS_2 Na hybrid, and (3) rolling the MoS_2 Na hybrid.[157] (b) Schematic diagram of the manufacturing process of the Na–Bi alloy foil. (c) The synthesis process of Na_3OCl/Na_3Bi@Na.[157] (d) The cyclic performance of symmetric batteries with bare Na, Na_3Bi@Na, and Na_3OCl/Na_3Bi@Na at 1.0 mA cm^{-2} and 1 mA h cm^{-2} (the inset was the schematic diagram of the Na_3OCl/Na_3Bi@Na anode).[155] (e and f) Schematic diagram of Na deposition model on the Na and Na/Bi composite anode.[156] (Reprinted with permission from ref. 157, 155 and 156. Copyright 2017 American Chemical Society, Copyright 2022 American Chemical Society and 2019 Wiley-VCH).

tion (Fig. 12e and f).[156] The high reduction of Na resulted in the formation of an Na–Bi alloy, and the electrode resistance dropped considerably following treatment. The Na/Bi–O_2 battery exhibited a discharge capacity of 1000 mA h g^{-1} over a cycle life of 50 cycles with a CE of 96.3%.

Similar to the usage of Na–Sn and Na–Bi alloy as the main material for SEI modification, the use of Na–Mo alloy has also been studied. Yang *et al.* used MoS_2 nanosheet to cover the surface of Na metal at room temperature to generate a composite SEI layer with Na_2S, MoS_2 and Mo (Fig. 12a).[157] The Na_2S created by the reaction could be widely disseminated on the surface of Na and used as a synthetic SEI film, inhibiting Na dendrite formation. The leftover MoS_2 nanoslice could form a 3D frame layer on the Na surface, efficiently accommodating the volume expansion throughout the Na deposition process. The symmetric cell with the composite SEI layer showed a low polarization voltage of 10 mV, which was much lower than that with the bare Na (31 mV) or the Na_2S-coated Na (90 mV) anodes.

3.2.3 Inorganic materials

3.2.3.1 Nonhalogen salt. The SEI layer rich in Na salt can induce the uniform deposition of Na^+ and reduce the formation of Na dendrites, effectively extending the battery cycle life. The artificial SEI layer rich in Na salt could be constructed on the surface of the Na anode by surface chemical treatment. Kumar *et al.* reported an artificial biphasic interphase (BPI) containing NaOH and $NaNH_3$ *via* the basic gas–solid two-phase reaction (Fig. 13a and b), followed by the specific chemical equation.[158]

$$2Na + 2H_2O \rightarrow 2NaOH + H_2$$

$$2Na + 2NH_3 \rightarrow 2NaNH_2 + H_2$$

The FESEM image revealed that the produced BPI (approximately 3 mm thick) could well cover the Na surface owing to the high stiffness and high ductility of the combined NaOH and $NaNH_3$. As shown in Fig. 13c and d, NaOH showed a strong Young's modulus of 31.0 GPa, while the $NaNH_3$ demonstrated stronger mechanical toughness, leading to a low Na^+ diffusion barrier during the sodium plating and stripping process. As a result, the Na/Na symmetric cell exhibited stable cycling performance for 500 cycles even at a high current density of 50 mA cm^{-2} (Fig. 13e and f). In comparison with the sharp death of the Na||S cell without BPI within 100 cycles, the BPI-Na||S cell showed an average CE of about 98.3% for over 500 cycles.

3.2.3.2 Halogen salt. NaF is the most used material for Na metal interface protection due to its excellent ionic conductivity and chemical inertness. Cheng *et al.* constructed a fluoride-based artificial SEI through the fluorination reaction between the $(C_2H_5)_3N(HF)_3$ fluorinating reagent and Na metal at room temperature.[159] It was found that the surface of the bare Na anode displayed irregular growth after Na deposition,

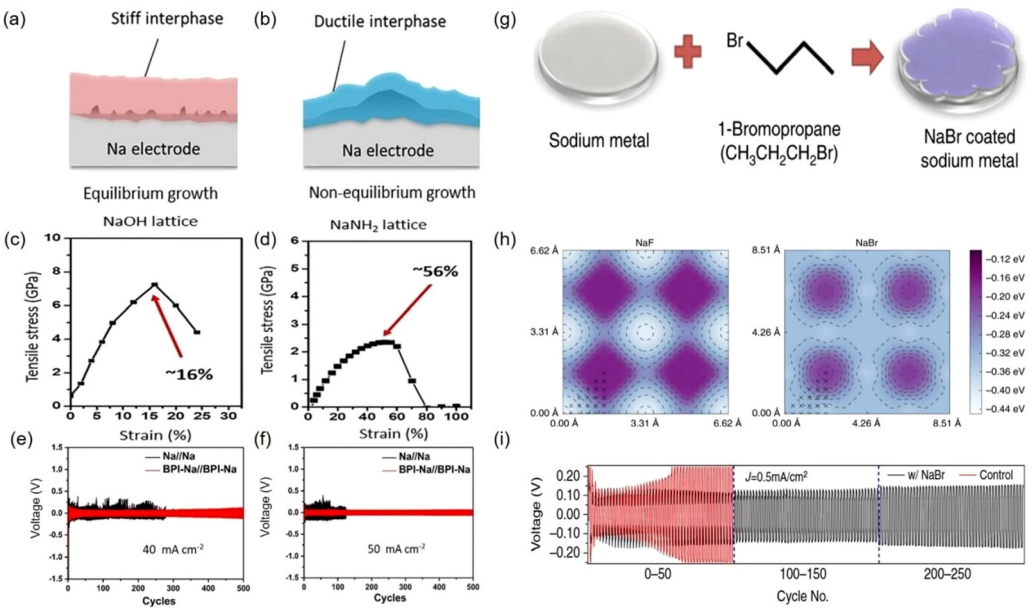

Fig. 13 (a and b) The schematic diagram of the surface on the Na anode showing the inhibition of large dendrite formation (due to the hardness interface of NaOH) and the regulation of large volume expansion during Na growth (due to the toughness of the $NaNH_2$ interface). The stress and strain responses of NaOH (c) and $NaNH_2$ (d) are calculated *via* DFT, respectively. The stripping/plating performance of symmetrical battery configurations with and without BPI at the current densities of (e) 40 mA cm^{-2} and (f) 50 mA cm^{-2}.[158] (f) Cycling stability of the symmetrical cell with/without the Na bromide layer. (g) Schematic diagram of the NaBr coating procedure. (h) The relationship between the surface binding energies of NaF (left) and NaBr (right) and the binding sites of adsorption atom diffusion by the joint density functional theory. (i) The voltage distribution current density obtained by continuously charging and discharging the symmetrical Na battery at 0.5 mA cm^{-2}.[61] (Reprinted with permission from ref. 61 and 158. Copyright 2020 The Author(s) and Copyright 2017 The Author(s)).

while the NaF-protected Na anode showed a smooth surface. Moreover, the assembled symmetrical batteries with NaF-based artificial SEI showed excellent long-cycle performance and small polarization. In addition, since the melting point of Na is 97.72 °C, it is also possible to achieve the NaF-rich SEI layer from the reaction between liquid Na metal and corresponding salts. Xu *et al.* added polytetrafluoroethylene (PTFE) powder into the molten Na metal to form an *in situ* NaF-rich SEI layer on the Na surface.[160] This protective layer had the potential to significantly limit the chemical activity of the Na surface. The symmetrical battery with the NaF@Na anode showed a low overpotential of ~8 mV at 1 mA cm^{-2} and excellent cycling stability even under rapid Na plating/stripping conditions at a current density of 10 mA cm^{-2}.

NaBr and NaCl, which have similar structure to NaF, are also widely concerned by researchers as components of artificial SEI membranes. Archer's research group reported that the low surface diffusion barrier of NaBr in the SEI layer was favorable for rapid Na^+ transport, resulting in the enhanced stability of the sodium deposition behavior.[61] The NaBr-based protective layer was formed *via* the chemical reaction of Na metal with bromopropane after evaporation (Fig. 13g). Compared to the diffusion barrier of NaF and other lithium salts, the diffusion barrier for NaBr was only about 0.02 eV per atom due to the large anion size, which was calculated using joint density functional theory (Fig. 13h). The symmetric sodium cell with NaBr-coated Na metal showed stable Na plating/stripping behavior at 0.5 mA cm^{-2} (Fig. 13i). The CE of the NaBr-coated Na||S cell remained almost unchanged for 250 cycles, but the blank Na||S cell failed almost immediately. Zhu *et al.* prepared a mixed SEI layer with NaCl, PhS_2Na_2, and Na_2S *via* the *in situ* reaction of *p*-dichlorobenzene and S_8 on the surface of Na anode.[161] The PhS_2Na_2-rich SEI layer showed a reduced binding energy (−2.3 eV) for Na^+, promoting uniform Na deposition behavior in the carbonate electrolyte. According to DFT calculations, the binding energy between the components of the SEI membrane generated in carbonate solvent (−3.515 eV, −2.497 eV, and −2.49 eV, respectively) had a small force, which may speed up Na^+ transport in PhS_2Na_2. A full battery assembled with a Prussia Blue (PB) cathode and bare Na anode displayed a capacity retention rate of only 50% after 1000 cycles, while the PhS_2Na_2-protected Na anode with an initial capacity of 89.5 mA h g^{-1} still had a capacity retention rate of 93% after 1000 cycles.

3.2.4 Organic polymers and their composites

3.2.4.1 Pure polymer. In addition to the inert inorganic material with high Na^+ conductivity, many researchers are interested in the studies of organic and organic–inorganic composite interphase protective layers on the surface of Na anode. Organic polymers with the merits of tailored functional groups and flexible structure are potential candidates for the modification of the artificial SEI layer, stabilizing the Na deposition/stripping process through the structural engineering of organic materials. The electrode and electrolyte can be effectively isolated by treating the surface of the Na anode with an organic polymer (such as polyvinylidene difluoride (PVDF), PTFE, and PEO) before assembling the battery. When the PVDF film with a repeating $-[CH_2CF_2]-$ monomer is prepared on the Cu collector and crystallized into structures with different F and H atom arrangements, which could form a PVDF-based protective layer on the Na surface after Na deposition.[32] Furthermore, PVDF can be utilized as the substrate to produce stable Na protective layers, promote Na^+ deposition, and limit the formation of Na dendrites. The PVDF@Cu electrode demonstrated an average CE of 99.48% for 1000 cycles at 2 mA cm^{-2} and 1 mA h cm^{-2}, while the cycle life of the blank Cu electrode was only 200 cycles with poor stability.

3.2.4.2 Coupling polymer and halogen salts. The SEI layer with high mechanical strength and excellent ionic conductivity could be constructed by the combination of organic polymers with Na salts. For example, Quan *et al.* developed a SEI membrane based on a mixture of PVDF and NaF (denoted as PNF@Cu).[162] The PVDF matrix could endure volume changes and retain the integrity of the anode coating interface, and the NaF particles boosted Na^+ diffusion conductivity and mechanical strength. The Young's modulus of PNF-mixed protective layer increased to 7.43 GPa, which was 3.5 times that of pure PVDF protective layer (Fig. 14a and b). The PNF-modified electrode showed a lower voltage polarization and a long-term cycle life for over 2000 h at 1 mA cm^{-2} in the symmetrical battery (Fig. 14c and d). Moreover, the PNF@Cu||FeS_2 full battery could retain more than 50% of its capacity after 350 cycles, while the PVDF@Cu||FeS_2 cell showed weak cycle stability and a quicker rate of capacity attenuation (Fig. 14e).

3.2.4.3 Coupling polymer and alloy. Furthermore, in view of the high ionic conductivity and strong chemical inertness of Na alloys, the SEI layer could be modified by the combination of organic molecules and Na alloy. Li *et al.* reported an organic–metal artificial layer containing PVDF and Bi on the Cu collector (PB@Cu), forming a sodiophilic alloyed Na_3Bi-phase and NaF-rich SEI layer after repeated Na plating/stripping.[163] The symmetrical cell with the PB@Cu electrode presented an ultralong cycle time of more than 2500 h and maintained a polarization voltage below 50 mV under the conditions of 1 mA cm^{-2} and 2 mA h cm^{-2} owing to the robust mechanical strength and high Na^+ conductivity of the artificial organic-metal interphase (Fig. 14g). In contrast, the symmetric cell with blank Cu showed an initial polarization voltage of 40 mV and rose quickly after 1000 h (Fig. 14f). The recent reported an *in situ* SEI and related approaches for promoting the cyclability of SMBs are shown in Table 4.

3.2.5 Artificial SEI layer between the SSEs and Na metal anodes

3.2.5.1 SEI layer on the Na anode. The manufactured SEI layer performs well in terms of reducing battery polarization and depositing Na^+ uniformly on the surface of Na metal. The main goal of creating an artificial SEI layer is to utilize its high ionic conductivity, consistent chemical performance, and uniform distribution to maintain the interphase stability between the Na anode and SSEs. In addition, using the fused Na could increase the contact area between the Na anode and the SSEs and decreased the voltage polarization as well.

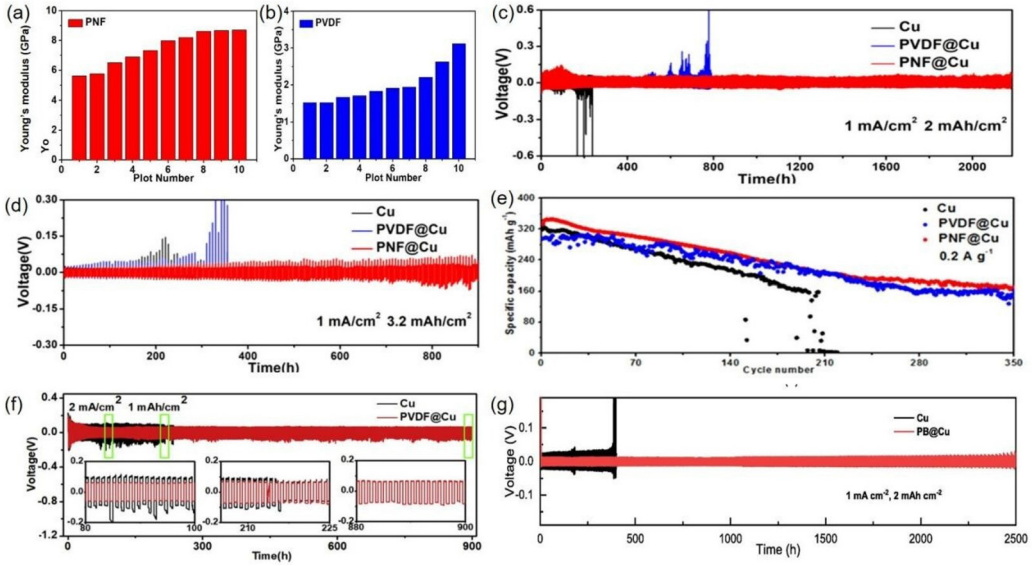

Fig. 14 (a and b) Young's modulus test of PNF and PVDF. (c and d) The cycle performance of the symmetrical battery with different treated electrodes at a current density of 1 mA cm^{-2} and area capacity of 2 mA h cm^{-2} and 3.2 mA h cm^{-2}, respectively. (e) Comparison of the cycle performance of Cu||FeS_2, PVDF@Cu||FeS_2, and PNF@Cu||FeS_2 at 0.2 A g^{-1}.[162] (f) The cycling performance of Na plating/stripping on Cu and PVDF@Cu current collectors at a cycling capacity of 1 mA h cm^{-2} at 2 mA cm^{-2}; (g) voltage profiles of symmetrical battery with bare Cu and PB@Cu collectors at 1 mA cm^{-2} with a fixed cycling capacity of 2 mA h cm^{-2}.[163] (Reprinted with permission from ref. 162 and 163. Copyright 2019 Elsevier B.V. and Copyright 2021 Elsevier B.V.).

Table 4 The comparison of the electrochemical performance of the Na metal electrode protected by the artificial SEI layer

Na@SEI	Electrolyte	Current density (mA cm^{-2})	Energy density (mA h cm^{-2})	Symmetrical battery (cycle life@ overpotential (mV))	Ref.
Na@NSCNTs	0.5 M NaTFSI + diglyme	1	1	500 h@70	31
Na@Al_2O_3(ALD)	$NaPF_6$ + diglyme	3	1	100 h@17	151
Na@Al_2O_3(PEALD)	1 M $NaClO_4$ + EC + DEC	0.25	—	450 h@100	152
Na@Na_xSn_y + NaCl	NaTFSI + diglyme	2	1	325 h@—	153
Na@Na-Bi	Carbonate-based electrolyte	1	1	500 h@20	154
Na@Na_3Bi + Na_3ClO	Carbonate-based electrolyte	1	1	700 h@30	155
Na@NaOH + $NaNH_3$	1 M NaTFSI + diglyme	1	1	1000 h@—	158
Na@NaF	1 M NaTFSI + diglyme	1	1	1000 h@8	160
		5	5	600 h@—	
Na@Na_2S + NaCl + R-S-Na + PhS_2Na_2	EC + PC	1	1	800 h@15	161
Na@PVDF	1 M $NaPF_6$ + diglyme	1	1	1200 h@35	32
Na@PVDF + NaF	1 M $NaPF_6$ + diglyme	1	2	900 h	162
		1	1	2100 h	
Na@Na_3Bi + PVDF	1 M $NaPF_6$ + diglyme	1	1	2700 h@35	163
		1	2	2500 h@—	

The Na/solid-state electrolyte interface can also be improved by the modification of Na anodes. Luo *et al.* added amorphous SiO_2 into Na metal to construct a Na–SiO_2 composite (Fig. 15a), which can reduce the surface tension and enhance the contact area between Na^+ superionic conductor (NASICON)-based SSEs and Na anode.[164] It was discovered that the interface resistance of Na||NASICON was 1658 Ω cm^{-2}, much more than that of the Na-SiO_2||NASICON (just 101 Ω cm^{-2}) in Fig. 15b. At a current density of 0.1 mA cm^{-2}, the original Na anode stopped working after 9 h, but the Na–SiO_2 composited anode showed a longer stability, indicating that reducing the interface resistance and enhancing the interface contact between the electrode and the electrolyte are crucial to the operation of SSEs (Fig. 15c). Cheng *et al.* annealed Na–K alloy to attach the carbon fiber at 750 °C to obtain the carbon-fiber-supported liquid Na–K alloy.[165] The carbon fiber would generate flaws on the structure after high temperature treatment, increasing its affinity with Na–K alloy (record as ZNSE). The alloy electrode and NASICON were joined at a pressure of 50 MPa, and the Na–K alloy was entirely bonded to the SSEs with no visible cracks or dendrites. At 1 mA cm^{-2}, the polarization voltage of Na–K||ZNSE||Na–K was much lower (which remained at 29 mV during cycles over 900 h) than that of Na||ZNSE||Na (which increased from 81 mV to 128 mV). The Na–K

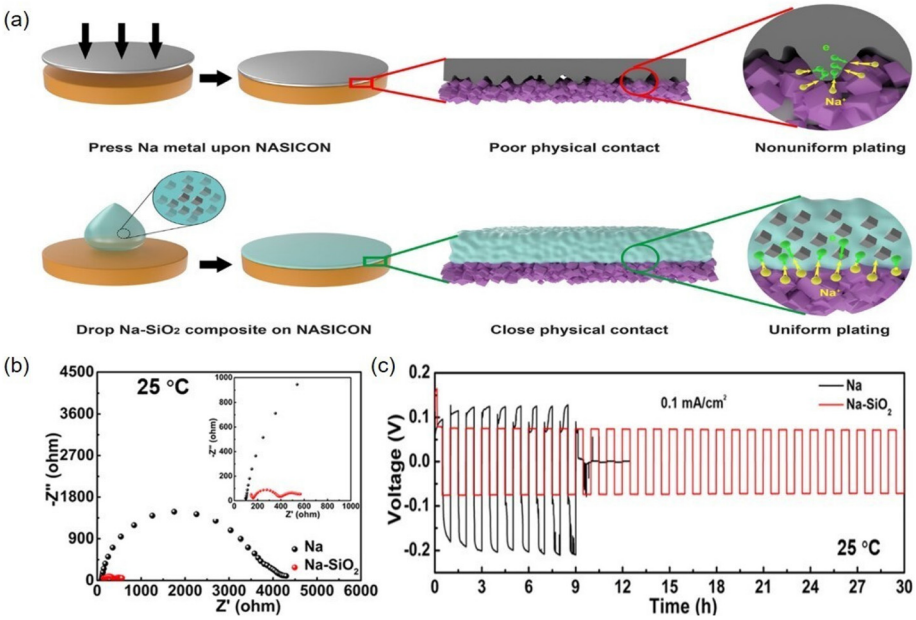

Fig. 15 (a) Contact schematic between the SSEs and Na or Na–SiO_2 electrode. (b) The impedance measurement of Na and Na–SiO_2-based battery. (c) The cycle performance of symmetrical cells using various electrodes at 0.1 mA cm^{-2}.[164] (Reprinted with permission from ref. 164. Copyright 2019 American Chemical Society).

alloy anode and NVP electrode were combined to make a whole battery that could cycle for more than 100 times under ideal conditions. Therefore, it is promising to improve the ionic conductivity and interface compatibility between SSEs and Na anode by modifying the surface of electrodes, thus promoting the practical applications of SSEs in SMBs.

3.2.5.2 SEI layer on SSEs. The solid–solid interface contact of the SSEs-based battery can be enhanced by the introduction of an artificial SEI layer on the surface of Na metal. Huang *et al.* proposed to remove the byproduct on the interface of $Na_3Zr_2Si_2PO_{12}$ (NZSP) under heat treatment to 450 °C, forming an interface layer composed of an Na^+-deficient surface (Fig. 16a).[166] It was found that the interface impedance of Na/NZSP (13 100 Ω cm^{-2}) was greater than that of Na/heat treated-NZSP (680 Ω cm^{-2}) (Fig. 16b). The reason is the development of Na^+ defects in NASP following high-temperature treatment. This defect can effectively improve the ion transfer efficiency on the solid–electrolyte surface and reduce the polarization of the full solid-state batteries (Fig. 16c).

Unlike oxide electrolytes, sulfide electrolytes will produce many side reactions with Na anodes on the interface; thus, the SEI layer prepared in sulfide SSEs needs to have certain chemical inertness to prevent the side reaction with sulfide from destroying its own structure. One of the solutions proposed by researchers is to add an interlayer between the SSE and the Na anode to improve the wettability and Na^+ conductivity of the interface. For example, molecular deposition technique (MLD) is used to produce an alucone film layer on the surface of Na anode.[167] A layer of alucone film was produced by 150 deposits on the surface of Na anode. The treated electrolyte was used to assemble a symmetrical battery to test its polarization. The Na@mld150C-Na_3SbS_4-Na@mld150C symmetrical battery could cycle for 475 h with a final polarization voltage of 450 mV. The polarization voltage of Na–Na_3SbS_4–Na battery increased to the value of 1.2 V from the initial 56 mV, with a cycle life of only 260 h. This method effectively separated the Na anode from the sulfide SSEs (Na_3SbS_4 and Na_3PS_4), preventing the breakdown of sulfide-based electrolytes and the formation of Na dendrites. This completely demonstrated that the alucone film had significant advantages in suppressing Na dendrite and stabilizing battery cycle performance.

Gerbaldi *et al.* developed a crosslinked polymer electrolyte (XPE) based on poly(ethylene oxide) (PEO) as the substrate, which was prepared by a solvent-free photopolymerization technique (Fig. 16d).[168] This XPE with $NaClO_4$ showed a high conductivity (>1 × 10^{-3} S cm^{-1}) at room temperature, and a passivation layer between the XPE and the electrode increasingly formed during the battery cycle. In the succeeding operation, this passivation layer will cause a modest rise in impedance and circulate steadily for 200 h (Fig. 16e). In addition, the therm gravimetric analysis test indicates that at high temperatures, the PC in the XPE volatilizes substantially less than that in the noncrosslinked electrolyte. Li *et al.* used IL electrolyte PYR14TFSI blended with NaTFSI (PYR/NaTFSI) as an effective interlayer to stabilize the interface of Na metal and sulfide SSE. This PYR/NaTFSI layer favored Na^+ transfer and solved the high interface resistance generated by the solid–solid contact.[169] When the current density was 0.1 mA cm^{-2}, the Na_3SbS_4-PYR/NaTFSI electrolyte in the symmetric cells can be used for stable cycling for 300 h, but the polarization voltage of the blank Na_3SbS_4 electrolyte suddenly dropped

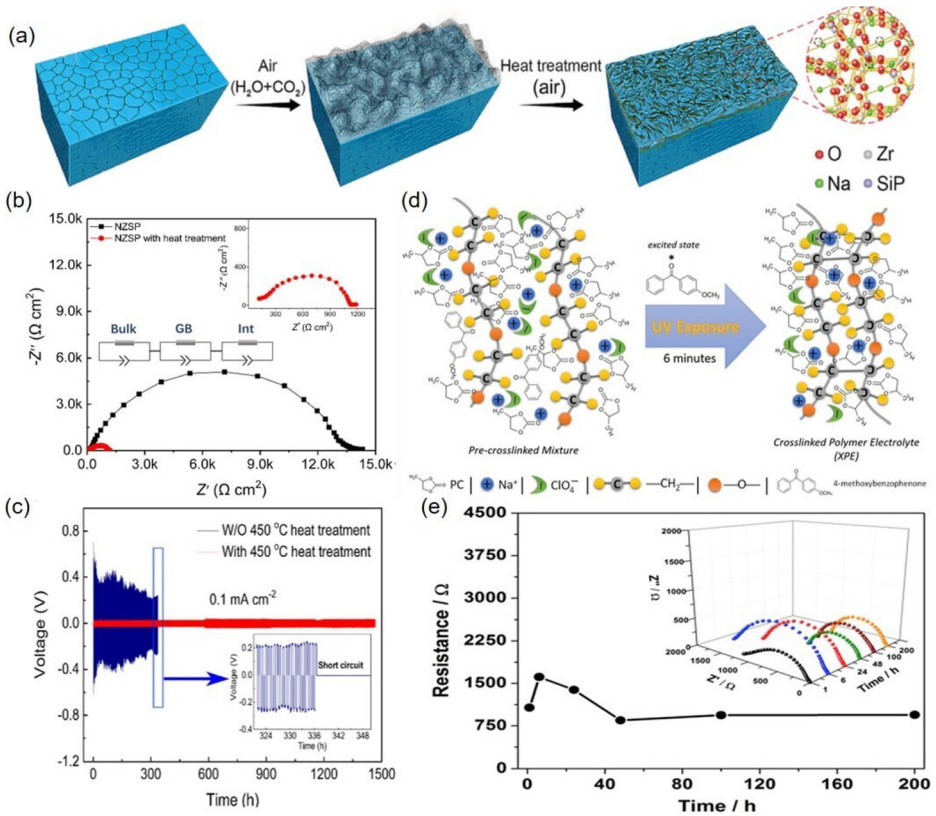

Fig. 16 (a) Schematic representation of how the NZSP surface structure changed in the presence of water (H_2O + CO_2) and elevated temperatures. (b) Evaluation of EIS schematics for symmetrical Na/NZSP/Na and Na/NZSP (heat treatment)/Na batteries. (c) Discharge/charge cycle analysis of symmetric Na/NZSP/Na and Na/NZSP (heat treatment)/Na batteries at 0.1 mA cm^{-2}.[166] (d) Diagrammatic representation of the anticipated reaction pathway for photoinduced crosslinking during XPE preparation. (e) The stability of the XPE interface in a symmetric Na/XPE/Na arrangement at room temperature. As seen in the illustration, the resistance number is taken from a single Nyquist diagram that the EIS measured.[168] (Reprinted with permission from ref. 166 and 168. Copyright 2020 American Chemical Society and Copyright 2017 Elsevier B.V.).

after 53 h, mainly owing to internal short circuit caused by Na dendrite formation.

3.3 3D conductive frameworks

The 3D conductive frameworks with open channels not only lessen volume growth of the Na metal during deposition but also lower the local current intensity to induce uniform Na^+ deposition on the frame, which prevents Na dendrite growth. There are various materials to the construction of a 3D conductive frame, including carbon-based frame,[170–173] metal and its oxide-based frame,[174–177] alloy-based frame, and MXene-based frame.[178–180]

3.3.1 Carbon-based frame. Carbon-based materials with high electrical conductivity and large specific surface area can promote homogeneous Na nucleation and deposition by lowering the local current densities. A mass of carbon-based materials, including graphene, carbon nanotubes, and carbon fiber, have undergone significant improvement as Na anode substrates, which demonstrated potential electrochemical characteristics in SMBs.

3.3.1.1 Carbon frame. Pure carbon materials are studied in detail in electrode processing, including carbon compounds such as carbon felt, carbon nanotubes, carbon nanowires, and carbon cloth, which are frequently used. Because of the exceptional thermal stability of carbon materials and the low melting point (97.72 °C) of Na metal, it is feasible to add liquid Na metal into carbon materials. As a result, liquid Na perfusion can be used in 3D electrical frames, and it could penetrate into the nanovoid of the 3D conductive frame through the capillary action. The electrode may gain the following benefits from this treatment: (1) a large numbers of nanogaps can efficiently hold the volume of Na anode during the cycle. (2) The formation of Na dendrites could be blocked by the increased surface area and the decreased current density.

Lee *et al.* developed a simple synthesis method by introducing nanocrevasses on the carbon fiber scaffold, which could make it easier for alkali metal penetrating into carbon cloth to improve the wettability of Na metal (Fig. 17a).[181] To put together, the initial Na electrode and Na/C electrode were used. The polarization of the symmetrical cells with bare Na anode increased after 10 h at a current density of 3 mA cm^{-2}, whereas the polarization of the Na/C anode in symmetrical cells did not substantially increase after 80 h. The Na/C anode

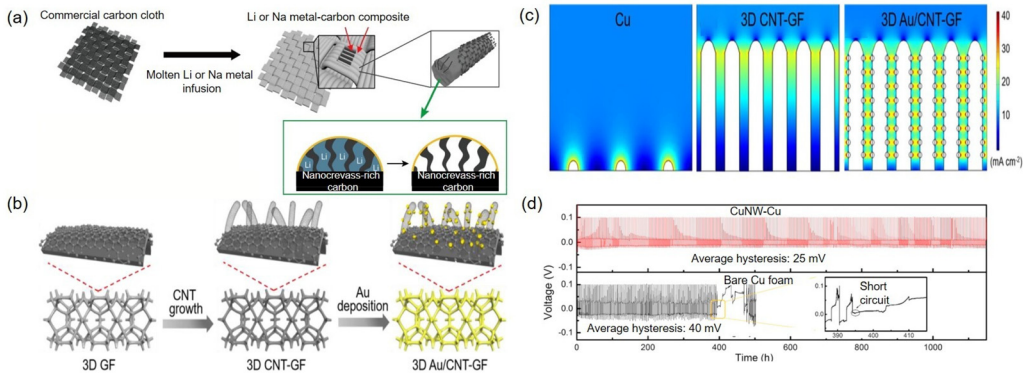

Fig. 17 (a) Schematic diagram of the manufacturing process of Li and Na metal/carbon composites.[181] (b) Schematic illustration of the preparation process of 3D Au/CNT-GF nanostructures. (c) The current density distribution on Cu, 3D CNT-GF, and 3D Au/CNT-GF electrodes simulated by COMSOL Multiphysics. (d) Polarization voltage curves of CuNW-Cu and bare Cu assembled asymmetrical cells.[63] (Reprinted with permission from ref. 181 and 63. Copyright 2019 American Chemical Society and Copyright 2022 Elsevier Ltd).

displayed a capacity of 1106 mA h g^{-1} and a capacity retain of 94.8%. In contrast, only 80.9% of the potential capacity (942.8 mA h g^{-1}) was released when bare Na foil was used. Fan *et al.* used commercial carbon felt as a feedstock by soaking it into the molten Na liquid to obtain Na/C composites, producing an electrode with great mechanical strength, electrochemical properties, good thermal stability, and substantial surface area.[33] As the carbon scaffold served as the site of Na deposition during the electrochemical cycle, Na plating and stripping capacities were kept constant at 2 mA h cm^{-2} in symmetrical cells. Symmetrical cells with bare Na demonstrated a large Na stripping/plating overpotential (>40 mV) and considerable irregular fluctuations throughout the cycle at 1 mA cm^{-2}. The Na/C composites not only displayed a significantly reduced overpotential (20 mV) but also attained stable cycle performance after 120 cycles, which even showed a small overpotential (50 mV) at 3 mA cm^{-2}. Besides, Yan *et al.* used 3D printing technology to prepare a reduced graphene oxide/carbon nanotube (rGO/CNT) microcrystalline aerogel with micropores and adjustable layered microcrystalline for Na metal host.[182] This rGO/CNT aerogel decreased the growth of Na dendrites and offered abundant active sites for Na deposition, facilitating the interface between the electrolyte and active ingredients, the penetration of the electrolyte into the nanostructures, and the ion transport rate. As a result, the CE of the main metal battery with rGO/CNT was maintained above 99%, while the initial CE of the blank Cu electrode in the symmetrical cell was only 48%, followed by a jump in the range of 83–100%.

3.3.1.2 Hybrid of metal and carbon materials. Based on 3D carbon materials, the reduced current density could result in a lower nucleation overpotential of Na metal, and the addition of another hybrid metal could further enhance the electrochemical stability for the SMBs. Wang *et al.* produced a 3D nanostructure composed of gold nanoparticles (Au-NPs) supported on a 3D carbon nanotube-graphene foam (3D CNT-GF) (Fig. 17b).[63] COMSOL multiphysics software was used to simulate the current density distribution on Cu, 3D CNT-GF, and 3D Au/CNT-GF electrodes to analyze the deposition behavior of Na on these electrodes (Fig. 17c). Dendrite formation during the surface deposition of Na^+ would be aided by the less concentrated sites on the two-dimensional copper foil. The CNT-GF electrode treated with Au had a lower current density and more nucleation sites than the original Cu electrode. The long-term cycle tests of the 3D Au/CNT-GF composite showed excellent cycle stability for more than 700 cycles with a CE of above 99%. In addition, the symmetrical cell with the 3D Au/CNT-GF electrode displayed an average polarization voltage of 25 mV (Fig. 17d). Besides, Wang *et al.* used Ag nanoparticles as active sites to modify CNT films to obtain the same effect as that of Au mentioned above.[183] The full battery with the Ag/CNT anode underwent 200 cycles after assembling with the NVP cathode, and the energy density remained at 90.1 mA h cm^{-2}.

To promote the uniform distribution of Na^+ on carbon-based materials, metal oxides can also be employed as active sites for Na deposition. Ye *et al.* used commercial carbon cloth (CC) modified by the concentrated nitric acid in $RuCl_3$ solution to obtain the lithiophilic CC layer containing RuO_2 nanoparticles (RuO_2@CC).[184] This Ru@CC layer showed good Na affinity during cycling, and the presence of RuO_2 particles could further limit the current density and impede dendrite formation of Na anode. The Na-Ru@CC electrode in the symmetrical battery showed stable voltage profile for over 250 h at 1 mA cm^{-2} with 1 mA h cm^{-2} in 1 M $NaClO_4$/EC with 5% FEC electrolyte, but the Na-Ru@CC electrode under the same conditions exhibited evident voltage fluctuations and sudden short-circuit at 58 h, originating from uneven plating/stripping on the surface of Na metal and severe dendritic growth.

3.3.1.3 Heteroatomic doped carbon materials. Carbon compounds may also be doped with nonmetallic atoms by the addition of metals. Zheng's research team discovered that N and O co-doped graphite carbon fiber (DGCF) matrix with evenly distributed dialkyl-functional groups helped to guide the uniform nucleation and growth of Na to form dendrite-free Na anodes.[185] With the wet chemical oxidation methods, a

number of strong negative functional groups (including N, ester groups (–COOR), carbonyl groups (–C═O), and hydroxyl groups (–OH)) could be introduced into the DGCF, which showed a definite negative charge due to more electronegative charges of nitrogen and oxygen than that of carbon. The DGCF-based symmetrical cell maintained a stable CE of 99.9% for 100 cycles at 1 mA cm^{-2} and 8 mA h cm^{-2}. Liu *et al.* treated cotton cloth at 900 °C in ammonia atmosphere to generate N, O-co-doped 3D carbon cloth frame to construct the porous 3D carbon fiber frame.[186] The symmetrical battery with the co-doped 3D carbon fiber frame displayed a 4.8 mV nucleation overpotential, and the Na@CC||NVP full battery maintained steady cycling performance throughout 100 cycles at a current density of 100 mA g^{-1}.

3.3.2 Alloy-based frame. Due to the weak mechanical strength of Na, it is challenging to guarantee the pristine appearance of the Na anode during the assembly procedure. In addition, the cycle stability of SMBs is decreased by the strong reactivity of Na metal. Alloys containing Na and other metals usually offer more stable chemical and electrochemical properties when compared to bare Na metal, and its mechanical strength will be significantly increased as well.

Li^+ is prone to gather near the negative surface because of its lower redox potential (−3.04 V *vs.* SHE) than Na (−2.71 V *vs.* SHE), which could form a strong electrostatic shielding effect to prevent dendritic growth during Na deposition on the Li–Na alloy anode (Fig. 18a).[187] The liquid Li–Na alloy instantly covered the carbon cloth (the Li/Na molar ratio was 2 : 1), creating a LiC6-based interfacial coating. The electrochemical behavior of LiNa-CC surfaces was distinct from that of Li and Na surfaces due to the eutectic melting of Li and Na alloy crystals, respectively (Fig. 18b and c). The symmetrical battery with a LiNa-CC-based anode demonstrated improved CE and superior electrochemical performance (maintained for 700 h cycles and a polarization voltage of 56 mV at 2 mA cm^{-2}) as compared to the blank Na anode, which had a lifetime of less than 150 turns (Fig. 18d and e). Liu *et al.* mechanically mixed $Na_{75}K$ alloy nanorods with PTFE particles, which underwent a cross-linking reaction during the mixing process, creating an Na metal anode with a 3D noncollapsing frame.[188] The nanostructured $Na_{75}K$ caused the defluorination of PTFE, leading to the formation of the crosslinked artificial SEI with NaF and KF. The PTFE@NaK//PTFE@NaK symmetric cell showed 60 mV micropolarization after 707 cycles, while the blank Na||Na symmetric cell exhibited an increased polarization voltage after the initial cycle and failed within 100 cycles.

The formation of Na dendrites can be reduced and the long-term cycling of SMBs can be promoted by the combination of alloy formation between alkali metals, in view of the electrostatic shielding effect and the reduction of current density. Besides the alloying between alkali metals, Na alloys with excellent properties can also be obtained using nonalkali metals. Huang *et al.* added a permeable ion/electron conductive framework *via* the reaction between molten Na and SnO_2, forming a percolated Na–Sn alloy/Na_2O framework (NSCA-31) on the Na metal (Fig. 19a and b).[189] The exposed "sodiophilic molecule" framework and its quick electron transport capabilities caused a uniform distribution of local current during the subsequent electroplating, which made it easier for Na^+ to deposit into the interior space while dampening the volume variations. The plating/stripping dynamics and stable interface of the NSCA-31 electrode (Na/SnO_2 weight ratio of 3 : 1) resulted in the resistance of the electrode remaining low and steady even after 50 cycles. It was clearly found that the treated electrode assembly had a smaller polarization and a longer cycle life than that of bare-Na assembled battery (Fig. 19c and d).

3.3.3 Metal and metal oxide-based frame. Chemically stable metals and metal oxides could make up the conductive framework as well, which ensures that Na^+ interacts with the metal framework during deposition. Wang *et al.* proposed a surface modification method for SMBs using copper nanowires formed on a 3D porous copper foam (CuNW-Cu) collector.[190] The application of Cu nanowires not only considerably increased the surface area of Cu foam but also decreased the local current density of uniform charge distribution by acting as functional nucleation sites and branching routes for Na^+. The entirely black CuNW-Cu indicated that the Cu foam underwent oxidation uniformly. The collector color would return to deep orange after the thermal reduction of CuO nanowires to Cu nanowires, indicating significant reduction. Assembled CuNW-Cu-based symmetrical batteries showed long-term cycles for more than 1200 h and an average polarization voltage of 25 mV. In contrast, the bare Cu electrode shorted at 390 h.

Moreover, Al is chosen as the candidate collector due to its high electrical conductivity and inert properties (Na is not

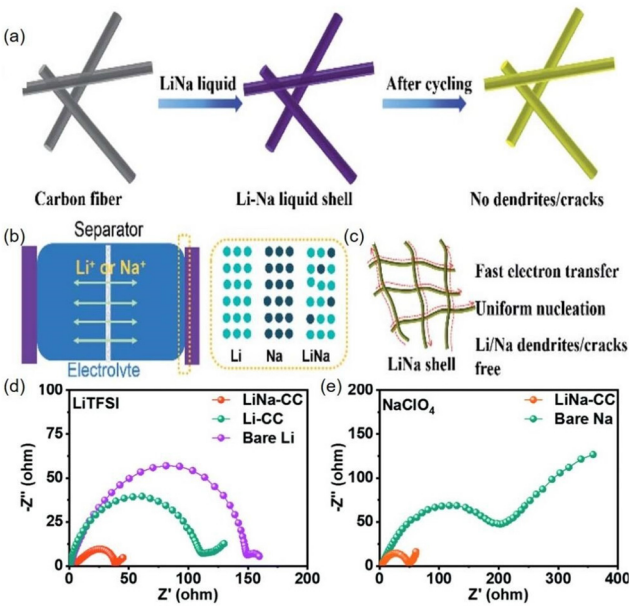

Fig. 18 (a) Schematic diagram of LiNa-CC anode preparation. (b) Schematic diagram of the symmetrical battery with various metal anodes. (c) The schematic illustration of liquid LiNa shell with enhanced electrochemical performance.[187] (Reprinted with permission from ref. 187. Copyright 2021 The Royal Society of Chemistry).

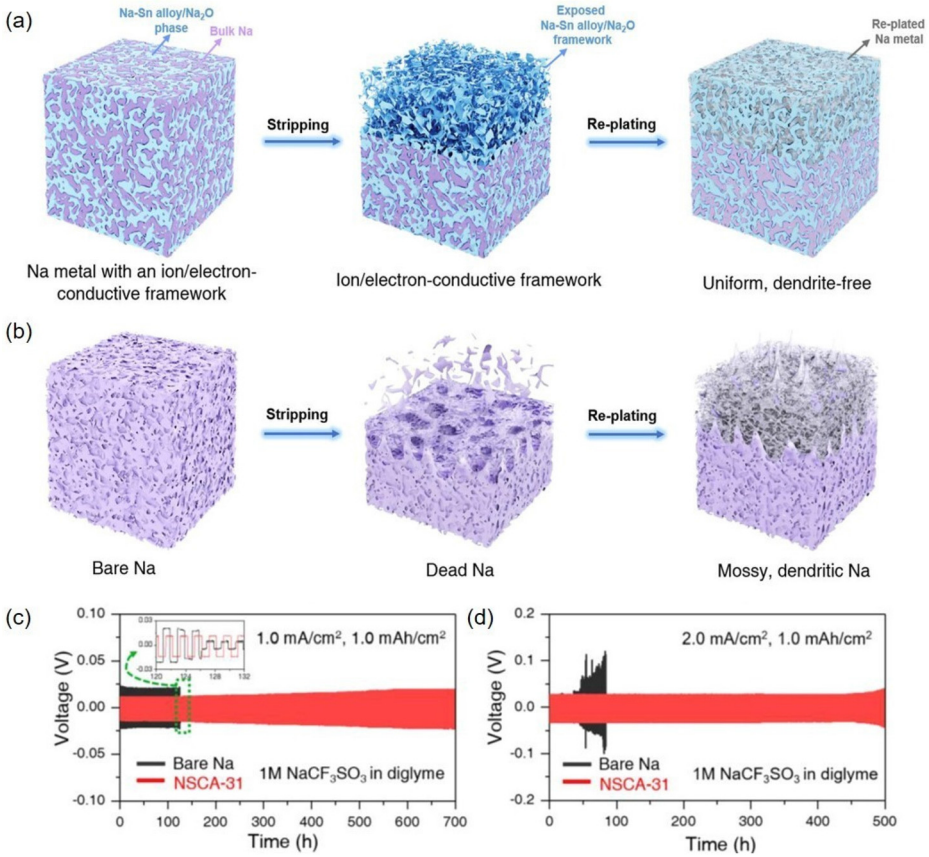

Fig. 19 Rapid and uniform Na^+ stripping and dendrite-free Na^+ plating on Na metals with ion/electron conductive frames. (b) Slow/uneven Na^+ stripping and dendritic Na^+ plating on bare Na metal. Cycling performance of symmetrical cells with bare Na and NSCA-31 electrodes with a capacity of 1.0 mA h cm^{-2} and the current densities of (c) 1.0 mA cm^{-2} and (d) 2.0 mA cm^{-2}.[189] (Reprinted with permission from ref. 189. Copyright 2019 Elsevier Ltd.).

alloyed with Al). Wang *et al.*[191] reported a porous Al collector as an electroplating substrate to inhibit Na dendrite growth. By reducing the distribution of Na flux and increasing the surface area available for Na nucleation, the interconnected porous structure may achieve uniform deposition. As a result, the Na anode with porous Al collector showed a steady plating/stripping performance for 1000 h, with an average CE of 99.9%. By contrast, the battery with the flat Al foil had a short circuit and a growing voltage lag. Besides, because Ni metal and Na metal have good bonding ability, it is also a good choice to use Ni metal to prepare a 3D frame for Na anode. Lu *et al.* used the mechanical rolling strategy to immerse Na metal in 3D Ni foam to obtain a 3D Ni/Na anode, which was favorable for decreasing the growth of Na dendrites caused by an excessive current density.[192] The 3D Ni/Na anode exhibited a polarization voltage of 13 mV and a stable cycle of 600 h at a current density of 1 mA cm^{-2}. In addition, the 3D Ni/Na anode could show a low polarization voltage of 38 mV at 3 mA cm^{-2}, and 3D Ni/Na||NVP full cells could stably cycled for more than 200 cycles with an initial capacity of 94 mA h g^{-1}.

Similarly, employing a metal oxide frame could also lower the surface current density to induce the uniform Na deposition and prevent the growth of Na dendrites. Li *et al.* reported the self-supported S–TiO_2 nanotube arrays *via* the electrochemical anodization and subsequent sulfidation process (Fig. 20c).[193] The S–TiO_2 tubular array has outstanding impedance characteristics when used as a binder-free electrode in an Na cell (Fig. 19d). The Na storage efficiency of S–TiO_2 can be attributed to its distinct nanotube array properties, significant doping effect on electronic properties, and enhanced dynamic stability. The S–TiO_2 nanotube with an outer diameter of 80 nm contributed to the even stripping/plating behavior of Na metal, enabling a long-term cycle stability (with a capacity retention of 91% after 4400 cycles) for the SMBs. The S–TiO_2 nanoarray electrode underwent a long-term test (Fig. 20e).

Yang *et al.* reported a 3D porous Cu foam containing ZnO nanorod arrays (CF@ZnO).[34] As shown in Fig. 20a, Na is typically sparsely distributed along the Cu ligaments' bones, particularly on their curved ridges. The irregular island architecture and high electric field distribution of the Na turning on bare Cu foam led to the gradual transformation of Na particles into Na dendrites and moss Na. The sodiophilic ZnO nanorod arrays on porous Cu form provided abundant nucleation sites

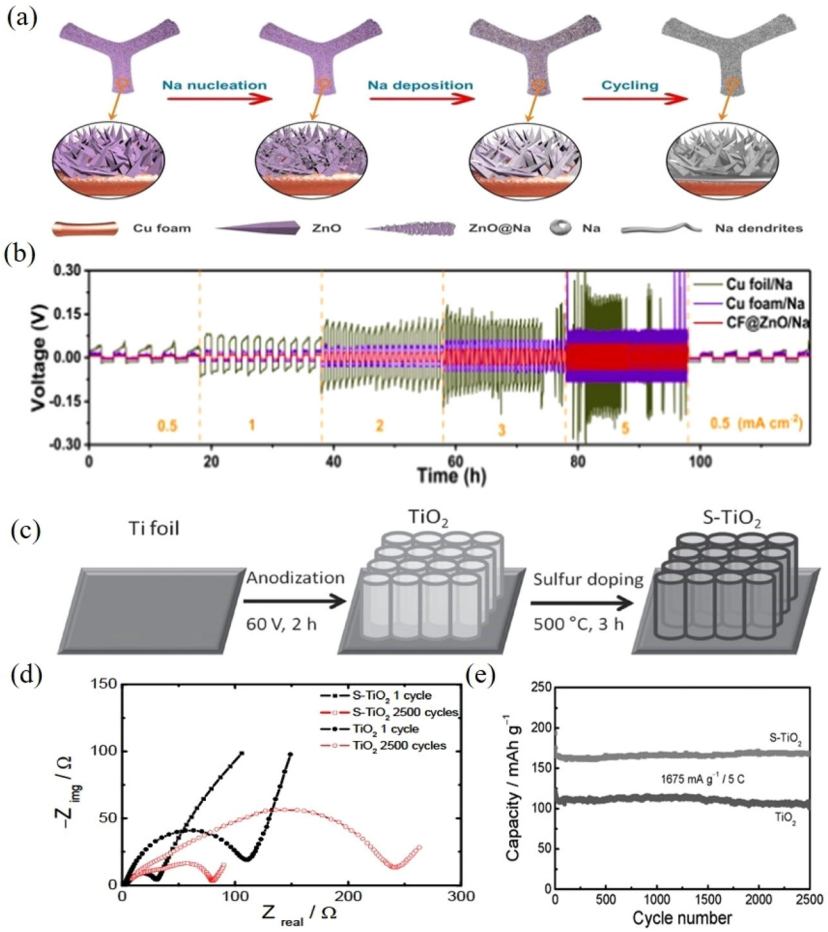

Fig. 20 (a) Schematic diagrams of Na nucleation and deposition on Cu foam (left) and CF@ZnO (right). (b) Rate performance of symmetric cells with different Na anodes.[34] (c) Electrochemical impedance spectra of S-TiO_2 and TiO_2 nanotube array anodes at different cycle stages. (d) The EIS spectra of the S-TiO_2 nanotube array assembled anode after 2500 cycles at 5 C. (e) Comparison of cycling performances of the S-TiO_2 nanoarray and TiO_2 electrodes at 5 C.[193] (Reprinted with permission from ref. 34 and 193. Copyright 2016 WILEY-VCH and Copyright 2020 Elsevier B. V.).

for Na metal, showing a low polarization voltage of 82 mV during deposition and stripping, whereas the untreated Na anode exhibited a higher polarization voltage of 207 mV than that of CF@ZnO. The full cell with CF@ZnO/Na anode delivered an outstanding rate capability, which showed that the CF@ZnO/Na anode could induce Na^+ deposition well.

3.3.4 MXene-based frame. MXene materials are two-dimensional inorganic compounds, which are composed of many atomic layer thick transition metal carbides, nitrides, or carbonitrides. MXene materials exhibit the metallic conductivity of transition metal carbides for the presence of hydroxyl or terminal oxygen on its surface.[194]

3.3.4.1 Hybrid of MXene and carbon. Mxene-based materials have certain electrical conductivity but poor adsorption of Na^+ due to their 3D layered materials. Therefore, researchers doped carbon materials with high ionic conductivity into MXene materials, which modified the carbon materials to increase Na nucleation sites on the surface and promote Na^+ deposition. Chen *et al.* reported a composite film of fibrous hydroxylated MXene and CNTs (h-Ti_3C_2/CNTs) *via* a simple vacuum filtration method (Fig. 21a), showing dendrite-free surfaces and insignificant volumes of the Na anode.[62] With the adsorption–desorption reaction, a huge number of O and F functional groups on the surface of h-Ti_3C_2/CNT engage strongly with Na atoms. The functional groups in hydroxylated h-Ti_3C_2/CNTs fiber could efficiently promote homogenous Na^+ deposition on the surface of the material. The h-Ti_3C_2/CNT/Na electrode showed a low polarization voltage of less than 50 mV before 200 h in the symmetrical battery, which could be kept below 110 mV even after cycling to 4000 h. Those using Na anodes failed within 100 cycles, and the bare Na and CNTs/Na electrodes showed large CE fluctuations during the cycle.

Moreover, the electrochemical properties of SMBs could be improved by the combination of MXene with carbon fiber. Cao *et al.* reported a MXene ($Ti_3C_2T_x$)-coated carbon cloth ($Ti_3C_2T_x$-CC) with high metal conductivity and sodiophilic surface.[195] The flexible Na-$Ti_3C_2T_x$-CC electrodes could be manufactured by a thermal infusion treatment in Fig. 21b. As a result, this Na-$Ti_3C_2T_x$-CC foil could be folded and rolled indefinitely, making it advantageous for use in flexible or irregularly

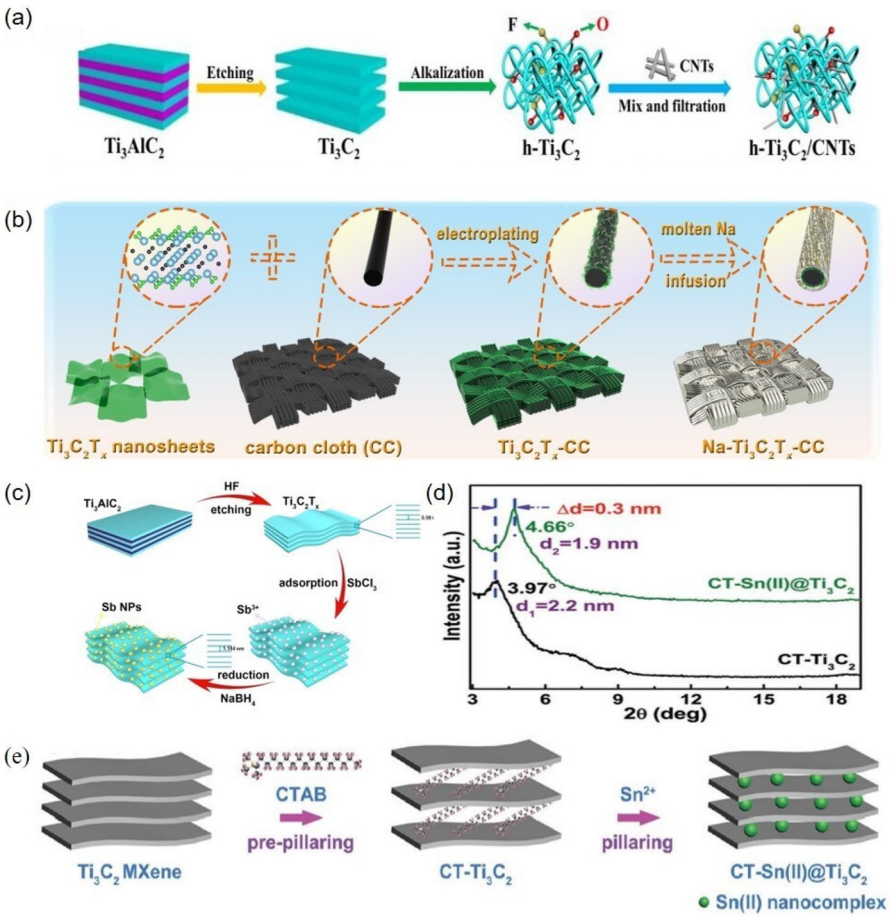

Fig. 21 (a) Schematic diagram of the synthesis route of h-Ti_3C_2/CNTs.[62] (b) Schematic diagram of the manufacturing procedures for the $Ti_3C_2T_x$-CC frame and Na-$Ti_3C_2T_x$-CC metal anode.[195] (c) Schematic illustration of the synthesis process of the $Ti_3C_2T_x$@Sb sample.[196] (d) XRD spectra of CT-Ti_3C_2 and CT-Sn(II)Ti_3C_2 before and after Sn^{2+} addition. (e) Schematic diagram of the preparation of CT-Sn(II)@Ti_3C_2 by CTAB pretreatment and Sn^{2+} column brace method.[198] (Reprinted with permission from ref. 62, 195, 196 and 198. Copyright 2020 Wiley-VCH, Copyright 2020 American Chemical Society, Copyright 2019 IOP Publishing Ltd and Copyright 2018 WILEY-VCH).

shaped batteries of flexible Na anodes. The $Ti_3C_2T_x$-CC induced uniform deposition and low interfacial resistance at 1.0 and 5.0 mA cm^{-2} current densities. The $Ti_3C_2T_x$-CC electrode showed a CE of 98.5% after 900 h, but the CC electrode showed a CE of 94% after cycling for 630 h.

3.3.4.2 Metal-doped MXene. The addition of metal ions on the surface of MXene materials could not only improve the interlayer spacing of MXene to accommodate more Na metal deposition but also induce Na^+ deposition in the MXene material interlayer. Du *et al.* reported the *in situ* modification of MXene with Sb nanoparticles ($Ti_3C_2T_x$@Sb) in Fig. 21c.[196] The MXene phase (Ti_3AlC_2) was immersed in HF (49%) solution at room temperature for 24 h to selectively etch the Al layer and replaced them with other surface groups such as –O, –OH, and –F. The mixed $Ti_3C_2T_x$@Sb-0.5 anode showed a long-term stability of 8000 cycles and provided a capacity of 148 mA h g^{-1} (with a capacity retention rate of 92.3%) at a high current density of 1 A g^{-1}, which proved that the addition of Sb nanoparticles played a positive role in the deposition of Na^+. Besides, Tian *et al.* treated Ti_3AlC_2 with HF to remove Al and then treated Ti_3C_2 with NaOH to increase the layer spacing of the multifunctional Mg(II)@Ti_3C_2 layer.[197] Through first-principles calculation, it could be concluded that Mg (0001) and Na (111) would form a good connection, making Mg a good nucleation site for Na^+ and promoting Na deposition. The Mg (II)@Ti_3C_2-modified Cu electrode showed good cycle stability and a high areal capacity of 2 mA h cm^{-2} in the SMBs. The Mg (II)@Ti_3C_2-modified Cu electrodes in full batteries showed a cycle life of 280 cycles and a high CE of 98.8%, but the Cu electrode showed unstable reaction from the initial cycle.

Furthermore, MXene with columnar morphology can also be effective to lower the current density and prevent Na dendrite formation. Li *et al.* reported Sn^{2+}-pillared Ti_3C_2 prefabricated by cetyltrimethylammonium bromide (CTAB) precolumnized with Ti_3C_2 (CT-Sn(II)@Ti_3C_2), which was used as a stable substrate for the dendrite-free Na metal anodes.[198] After CTAB pretreatment, the layer spacing of Ti_3C_2 was increased to 2.2 nm, indicating that CTAB was successfully embedded between Ti_3C_2 layers. No additional peaks were observed in the XRD spectra of CT-Sn(II)@Ti_3C_2 after Sn^{2+} columned,

suggesting the presence of amorphous intercalated Sn(II) nanocomplexes in the CT-Ti_3C_2 matrix (Fig. 21d). In addition, the CT-Sn(II)@Ti_3C_2 electrode could still obtain a high CE of 98.8% under a current density of 5 mA cm^{-2} and an areal capacity of 5 mA h cm^{-2}. Impressively, CT-Sn(III)@Ti_3C_2 was able to provide a high CE of 98.5% after 100 cycles even at 10 mA cm^{-2}, further demonstrating the positive impact of Sn^{2+} inserted between Ti_3C_2 layers on Na nucleation and deposition behavior.

3.3.4.3 Hybrid of MXene and polymers. Furthermore, in view of the merits of the flexible structure and functional designability, polymers can also be mixed with MXene to promote the deposition behavior and cycle stability of Na metal anode. Zhang *et al.* prepared the co-doped poly(vinylidene fluoride hexafluoropropylene) (PVDF-HFP) functional gel polymer electrolyte (GPE) through weak hydrogen bond interaction using polyethylene glycol 4000 (PEG-4000) and conductive Ti_3C_2 (MXene), which was denoted as PHPM.[199] The ionic conductivity of this PHPM electrolyte could reach 1.76×10^{-3} S cm^{-1}. The addition of MXene material in PHPM electrolyte could improve the Na^+ transport rate and effectively suppress the formation of Na dendrites. The Na/PHPM/Na symmetric cell exhibited a polarization voltage of 168 mV and stable deposition performance for 1200 h at 5 mA cm^{-2}. By contrast, the overpotential of the Na/GPE/Na symmetric cell with PVDF-HFP GPE gradually increased and finally reached 1.3 V after 1000 h of cycling. The electrochemical properties of PVDF-HFP, PHP, and PHPM GPE were also evaluated in a sodium metal battery with a titanium phosphate sodium cathode. The specific discharge capacity of the PVDF-HFP-based cell (97.2 mA h g^{-1}) after 300 cycles was much lower than that of the PHP (112.0 mA h g^{-1}) and PHPM (117.5 mA h g^{-1}) systems.

In summary, the surface current density can be greatly decreased by incorporating a 3D conductive frame into the Na anodes, and the reduction in the current density successfully causes the uniform deposition of Na^+. In addition, adding Na^+ nucleation sites to the 3D frame or enhancing the sodiophilic surface of the 3D structure can enhance the battery performance as well.

4. Conclusion and perspective

Because of its high theoretical capacity, low realizable redox potential, and abundant supplies, Na metal is regarded as a viable anode material for high-energy-density SMBs. Uncontrollable Na dendrite formation and excessive volume fluctuation result in low CE, poor cycle performance, and even serious safety issues for Na metal anodes, limiting the practical application of SMBs. The structure/interface engineering on Na metal anode is emerging to regulate Na plating/stripping process and improve the cycling stability of SMBs. This review concentrates on three aspects of anodic protection: (1) *in situ* SEI with electrolyte additives; (2) artificial SEI modification; (3) a 3D conductive frame structure. The strategies of constructing even and stable SEI membrane are usual to promote the uniform deposition of Na^+ and suppress the side reactions between Na and electrolyte, boosting CE and cycling stability of SMBs. The porous structure of 3D frameworks has been shown to be effective to decrease the volume expansion of Na anodes, resulting in enhanced cycling stability and the whole electrochemical performance of SMBs.

Although Na metal anode has achieved amazing progress so far, there are still several obstacles in this field, including low CE, poor cycling stability, and limited energy density. This review puts forward the promising development prospects and research directions for Na anode protection, promoting the further applications of SMBs in practical large-scale energy storage devices. As an outlook, the structure/interface engineering on Na metal anode of SMBs can be further improved through the following aspects.

(1) Firstly, the formation mechanism and evolution process of Na dendrites should be deeply analyzed and monitored with high-resolution characterization techniques and advanced theoretical calculations. In particular, *in situ* characterization techniques (*i.e.*, cryo-electron microscopy, high-resolution TEM, and TOF-SIMS) are promising tools to resolve the dendritic dilemma, speeding up the data analysis process of structural/interfacial changes of Na metal anodes. Moreover, the emerging machine learning methods should be used to illustrate the Na dendrite evolution mechanisms in the near future.

(2) Secondly, the types of anodes for SMBs should be expanded and explored, and the related issues should be taken into consideration as well. For instance, the alloy-based electrode may be served as a potential replacement for a new generation of high-energy-density anodes. The composited anodes not only reduce the volume change but also increase the electronic conductivity. The utilization of polymer or hybrid organic and inorganic electrode materials offers significant potential for high safety batteries. Nevertheless, the mechanism of Na^+ exfoliation and deposition in polymers and organic/inorganic interfaces requires additional investigation.

(3) Thirdly, the modification and optimization of the SEI layer should consider the components and structures of electrolytes, cathode, and anode, which are crucial parameters for constructing uniform SEI layers. Strategies introducing *in situ* SEI with electrolyte additives and constructing artificial SEI layer put promote the ion transfer rate and uniformity of ion distribution on the Na metal surface. Notably, atomic/molecular layer deposition methods could be effective ways for producing high-quality SEI films, which can provide a controlled surface protective layer.

(4) Fourthly, the accessible surface area of the 3D frame causes significant Na and electrolyte consumption during the repeated deposition and peeling of Na^+ in the 3D frame. Na metal still contacts the electrolyte while being enclosed in the matrix. To effectively increase the stability of the Na anode, the protective coating must be formed on the surface of the three-dimensional structures. The combination of SEI modification and 3D frame may open up an avenue toward high-performance SMBs with enhanced stability.

(5) Fifthly, the construction of 3D conductive frameworks should take the gravity and volume energy densities into account, which may affect the actual energy density of the whole battery. The obtained electrode cannot make full use of the energy density of its volume and weight in practical applications at present, and the weight and volume of the designed framework and Na should be optimized. The quantitative relationship between the effects of Na dendrite suppression and the whole energy density of the SMBs need to be further studied.

Moreover, SSEs are proposed to address the electrolyte loss and safety issues of the traditional liquid electrolytes of SMBs. However, the initial solid–solid interface of SSEs causes an increase in the interface impedance, leading to declining CE and increasing polarization in the SSE-based SMBs. Notably, the interface compatibility of SSEs could be improved by the methods of SEI modification, structural transformations of SSEs, enhanced interfacial contact between SSEs and Na metal, *etc*. Therefore, the further exploration and structural design of SSEs with high ionic conductivity, well-interfaced compatibility, and high safety are effective means to promote the commercial application of SMBs.

As for the industrialization development trend of SMBs, cost is the main benefit of Na metal batteries over Li metal batteries. Firstly, compared to Li metal, Na metal is more widely distributed in the crust, which results in a lower price for Na metal anode. Secondly, Al foil can be used as the current collector in SMBs, which is less expensive than that of the Cu collector in Li metal batteries. Theoretically, SMBs have a higher energy density than sodium ion batteries, and they will have a wider range of potential applications in the future. Due to the rising popularity of electric vehicles, cost control will eventually become a significant barrier to the development of Li metal/ion batteries. Na metal/ion batteries can store more raw materials than Li metal/ion batteries, which provides a structural foundation for next-generation electric vehicles and future large-scale electrical storage. In addition, the Na metal/ion battery-powered devices could be used in conjunction with Li metal/ion battery-powered devices, which lowers the cost of enterprise transformation and encourages the manufacturing of SMBs.

In addition, in the field of low temperature batteries, it is also one of the advantages of the future industrialization of Na ion/metal batteries. Compared with Li ion/metal battery, the solvation energy and transport barrier of Na^+ in the electrolyte are smaller than those of Li^+, which could enable Na ion/metal batteries with higher coulombic efficiency at lower temperatures. In the field of low-temperature batteries, the minimum operating temperature of Li-ion batteries is −20 °C, while Na-ion batteries can work normally at a low temperature of −40 °C. This provides a solution for the application of low-temperature batteries in the future and the demand for batteries in some extreme environments, which will promote the industrialization of Na ion/metal batteries in the future.

Nevertheless, the electrolyte formula has a significant impact on electrode protection across the entire battery system. More comparative studies between ester and ether electrolytes should be added in the upcoming study of electrolyte formula. Comparative studies help to improve the mix of new electrodes and electrolyte solutions and to produce more stable and effective battery cycles, which could provide in-depth strategies to promote further commercial applications of SMBs.

Conflicts of interest

The authors declare no competing financial interests.

Acknowledgements

This work was supported by Joint Fund of Science and Technology R&D Plan of Henan Province (222301420005), the National Natural Science Foundation of China (U22A20437, 21773055), Key Scientific Research Project of Higher Education in Henan Province (22A150004), and China Postdoctoral Science Foundation under Grant (2021M701069).

References

1 G. E. Blomgren, *J. Electrochem. Soc.*, 2017, **164**, A5019–A5025.
2 A. Yoshino, *Angew. Chem., Int. Ed.*, 2012, **51**, 5798–5800.
3 B. Scrosati, *J. Solid State Electrochem.*, 2011, **15**, 1623–1630.
4 M. Armand and J.-M. Tarascon, *Nature*, 2008, **451**, 652–657.
5 H. Pan, Y.-S. Hu and L. Chen, *Energy Environ. Sci.*, 2013, **6**, 2338.
6 S.-W. Kim, D.-H. Seo, X. Ma, G. Ceder and K. Kang, *Adv. Energy Mater.*, 2012, **2**, 710–721.
7 H. Ryu, T. Kim, K. Kim, J.-H. Ahn, T. Nam, G. Wang and H.-J. Ahn, *J. Power Sources*, 2011, **196**, 5186–5190.
8 T. H. Hwang, D. S. Jung, J.-S. Kim, B. G. Kim and J. W. Choi, *Nano Lett.*, 2013, **13**, 4532–4538.
9 S. Xin, Y. X. Yin, Y. G. Guo and L. J. Wan, *Adv. Mater.*, 2014, **26**, 1261–1265.
10 A. Manthiram and X. Yu, *Small*, 2015, **11**, 2108–2114.
11 W. Liu, Q. Sun, Y. Yang, J.-Y. Xie and Z.-W. Fu, *Chem. Commun.*, 2013, **49**, 1951–1953.
12 P. Hartmann, C. L. Bender, M. Vracar, A. K. Durr, A. Garsuch, J. Janek and P. Adelhelm, *Nat. Mater.*, 2013, **12**, 228–232.
13 C. Xia, R. Black, R. Fernandes, B. Adams and L. F. Nazar, *Nat. Chem.*, 2015, **7**, 496–501.
14 M. Geng, D. Han, Z. Huang, S. Wang, M. Xiao, S. Zhang, L. Sun, S. Huang and Y. Meng, *Energy Storage Mater.*, 2022, **52**, 230–237.
15 A. P. V. K. Saroja and Y. Xu, *Matter*, 2022, **5**, 808–836.
16 X. L. Huang, Y.-X. Wang, S.-L. Chou, S. X. Dou and Z. M. Wang, *Energy Environ. Sci.*, 2021, **14**, 3757–3795.

17 X. L. Huang, S. X. Dou and Z. M. Wang, *Mater. Horiz.*, 2021, **8**, 2870–2885.
18 F. Croce, G. B. Appetecchi, L. Persi and B. Scrosati, *Nature*, 1998, **394**, 456–458.
19 D. Aurbach, *Solid State Ionics*, 2002, **148**, 405–416.
20 C. Monroe and J. Newman, *J. Electrochem. Soc.*, 2005, **152**, A396–A404.
21 L. Suo, Y. S. Hu, H. Li, M. Armand and L. Chen, *Nat. Commun.*, 2013, **4**, 1481.
22 G. Zheng, S. W. Lee, Z. Liang, H. W. Lee, K. Yan, H. Yao, H. Wang, W. Li, S. Chu and Y. Cui, *Nat. Nanotechnol.*, 2014, **9**, 618–623.
23 M. S. Park, S. B. Ma, D. J. Lee, D. Im, S.-G. Doo and O. Yamamoto, *Sci. Rep.*, 2014, **4**, 3815.
24 W. Xu, J. Wang, F. Ding, X. Chen, E. Nasybulin, Y. Zhang and J.-G. Zhang, *Energy Environ. Sci.*, 2014, **7**, 513–537.
25 J. Qian, W. A. Henderson, W. Xu, P. Bhattacharya, M. Engelhard, O. Borodin and J. G. Zhang, *Nat. Commun.*, 2015, **6**, 6362.
26 Y. Lu, Z. Tu and L. A. Archer, *Nat. Mater.*, 2014, **13**, 961–969.
27 W. Luo, L. Zhou, K. Fu, Z. Yang, J. Wan, M. Manno, Y. Yao, H. Zhu, B. Yang and L. Hu, *Nano Lett.*, 2015, **15**, 6149–6154.
28 M.-H. Ryou, D. J. Lee, J.-N. Lee, Y. M. Lee, J.-K. Park and J. W. Choi, *Adv. Energy Mater.*, 2012, **2**, 645–650.
29 J. S. Kim, D. J. Yoo, J. Min, R. A. Shakoor, R. Kahraman and J. W. Choi, *Chem. Nanomater.*, 2015, **1**, 240–245.
30 Y.-J. Kim, H. Lee, H. Noh, J. Lee, S. Kim, M.-H. Ryou, Y. M. Lee and H.-T. Kim, *ACS Appl. Mater. Interfaces*, 2017, **9**, 6000–6006.
31 B. Sun, P. Li, J. Zhang, D. Wang, P. Munroe, C. Wang, P. H. L. Notten and G. Wang, *Adv. Mater.*, 2018, **30**, 1801334.
32 Z. Hou, W. Wang, Y. Yu, X. Zhao, Q. Chen, L. Zhao, Q. Di, H. Ju and Z. Quan, *Energy Storage Mater.*, 2020, **24**, 588–593.
33 S. S. Chi, X. G. Qi, Y. S. Hu and L. Z. Fan, *Adv. Energy Mater.*, 2018, **8**, 1702764.
34 W. Yang, W. Yang, L. Dong, G. Shao, G. Wang and X. Peng, *Nano Energy*, 2021, **80**, 105563.
35 X. Chi, F. Hao, J. Zhang, X. Wu, Y. Zhang, S. Gheytani, Z. Wen and Y. Yao, *Nano Energy*, 2019, **62**, 718–724.
36 D. I. Iermakova, R. Dugas, M. R. Palacín and A. Ponrouch, *J. Electrochem. Soc.*, 2015, **162**, A7060–A7066.
37 N. Yabuuchi, K. Kubota, M. Dahbi and S. Komaba, *Chem. Rev.*, 2014, **114**, 11636–11682.
38 R. Rodriguez, K. E. Loeffler, S. S. Nathan, J. K. Sheavly, A. Dolocan, A. Heller and C. B. Mullins, *ACS Energy Lett.*, 2017, **2**, 2051–2057.
39 X. Chen, X. Shen, B. Li, H. J. Peng, X. B. Cheng, B. Q. Li, X. Q. Zhang, J. Q. Huang and Q. Zhang, *Angew. Chem., Int. Ed.*, 2018, **57**, 734–737.
40 C. Brissot, M. Rosso, J. N. Chazalviel, P. Baudry and S. Lascaud, *Electrochim. Acta*, 1998, **43**, 1569–1574.
41 M. Rossoa, T. Gobron, C. Brissot, J. N. Chazalviel and S. Lascaud, *J. Power Sources*, 2001, **97–98**, 804–806.
42 R. Zhang, X. B. Cheng, C. Z. Zhao, H. J. Peng, J. L. Shi, J. Q. Huang, J. Wang, F. Wei and Q. Zhang, *Adv. Mater.*, 2016, **28**, 2155–2162.
43 I. W. Seong, C. H. Hong, B. K. Kim and W. Y. Yoon, *J. Power Sources*, 2008, **178**, 769–773.
44 B. Sun, P. Xiong, U. Maitra, D. Langsdorf, K. Yan, C. Wang, J. Janek, D. Schroder and G. Wang, *Adv. Mater.*, 2020, **32**, e1903891.
45 H. J. Yoon, N. R. Kim, H. J. Jin and Y. S. Yun, *Adv. Energy Mater.*, 2018, **8**, 1701261.
46 X. Hu, P. H. Joo, H. Wang, E. Matios, C. Wang, J. Luo, X. Lu, K. Yang and W. Li, *Adv. Funct. Mater.*, 2019, **29**, 1807974.
47 Z. Chen, J. Cao, X. Wu, D. Cai, M. Luo, S. Xing, X. Wen, Y. Chen, Y. Jin, D. Chen, Y. Cao, L. Wang, X. Xiong and B. Yu, *ACS Appl. Mater. Interfaces*, 2022, **14**, 12223–12233.
48 R. L. Sacci, J. M. Black, N. Balke, N. J. Dudney, K. L. More and R. R. Unocic, *Nano Lett.*, 2015, **15**, 2011–2018.
49 Y. Zhao, X. Yang, L.-Y. Kuo, P. Kaghazchi, Q. Sun, J. Liang, B. Wang, A. Lushington, R. Li, H. Zhang and X. Sun, *Small*, 2018, **14**, 1703717.
50 X. Liang, Q. Pang, I. R. Kochetkov, M. S. Sempere, H. Huang, X. Sun and L. F. Nazar, *Nat. Energy*, 2017, **2**, 17119.
51 Y. Zhang, J. Qian, W. Xu, S. M. Russell, X. Chen, E. Nasybulin, P. Bhattacharya, M. H. Engelhard, D. Mei, R. Cao, F. Ding, A. V. Cresce, K. Xu and J. G. Zhang, *Nano Lett.*, 2014, **14**, 6889–6896.
52 F. Ding, W. Xu, G. L. Graff, J. Zhang, M. L. Sushko, X. Chen, Y. Shao, M. H. Engelhard, Z. Nie, J. Xiao, X. Liu, P. V. Sushko, J. Liu and J. G. Zhang, *J. Am. Chem. Soc.*, 2013, **135**, 4450–4456.
53 X. B. Cheng, T. Z. Hou, R. Zhang, H. J. Peng, C. Z. Zhao, J. Q. Huang and Q. Zhang, *Adv. Mater.*, 2016, **28**, 2888–2895.
54 J. Zhang, G. Cai, D. Zhou, H. Tang, X. Wang, C. Gu and J. Tu, *J. Mater. Chem. C*, 2014, **2**, 7013–7021.
55 M. Wu, Z. Wen, Y. Liu, X. Wang and L. Huang, *J. Power Sources*, 2011, **196**, 8091–8097.
56 J. Yang, A. Kraytsberg and Y. Ein-Eli, *J. Power Sources*, 2015, **282**, 294–298.
57 D. Lin, Y. Liu, Z. Liang, H.-W. Lee, J. Sun, H. Wang, K. Yan, J. Xie and Y. Cui, *Nat. Nanotechnol.*, 2016, **11**, 626–632.
58 C. Jin, O. Sheng, J. Luo, H. Yuan, C. Fang, W. Zhang, H. Huang, Y. Gan, Y. Xia, C. Liang, J. Zhang and X. Tao, *Nano Energy*, 2017, **37**, 177–186.
59 A. O. Raji, S. R. Villegas, N. D. Kim, X. Fan, Y. Li, G. Silva, J. Sha and J. M. Tour, *ACS Nano*, 2017, **11**, 6362–6369.
60 Z. W. Seh, J. Sun, Y. Sun and Y. Cui, *ACS Cent. Sci.*, 2015, **1**, 449–455.
61 S. Choudhury, S. Wei, Y. Ozhabes, D. Gunceler, M. J. Zachman, Z. Tu, J. H. Shin, P. Nath, A. Agrawal, L. F. Kourkoutis, T. A. Arias and L. A. Archer, *Nat. Commun.*, 2017, **8**, 898.

62 X. He, S. Jin, L. Miao, Y. Cai, Y. Hou, H. Li, K. Zhang, Z. Yan and J. Chen, *Angew. Chem., Int. Ed.*, 2020, **59**, 16705–16711.
63 Z. Huang, Z. Wang, B. Tian, T. Xu, C. Ma, Z. Zhang, J. Zang, D. Kong, X. Li and Y. Wang, *J. Mater. Sci. Technol.*, 2022, **118**, 199–207.
64 J. Lv, H. Sun, Z. Sun, C. Ding and W. Huang, *J. Mater. Chem. A*, 2022, **50**, 324–331.
65 H. Che, S. Chen, Y. Xie, H. Wang, K. Amine, X.-Z. Liao and Z.-F. Ma, *Energy Environ. Sci.*, 2017, **1**, 1075–1101.
66 W. Zhang, F. Zhang, F. Ming and H. N. Alshareef, *Energy Chem.*, 2019, **1**, 100012.
67 Y. Sun, P. Shi, H. Xiang, X. Liang and Y. Yu, *Small*, 2019, **15**, 1805479.
68 Y. Fang, L. Xiao, Z. Chen, X. Ai, Y. Cao and H. Yang, *Electrochem. Energy Rev.*, 2018, **1**, 294–323.
69 A. Ponrouch, D. Monti, A. Boschin, B. Steen, P. Johansson and M. R. Palacin, *J. Mater. Chem.*, 2015, **3**, 22–42.
70 R. Fong, U. von Sacken and J. R. Dahn, *J. Electrochem. Soc.*, 1990, **137**, 2009–2013.
71 C. Zhong, Y. Deng, W. Hu, J. Qiao, L. Zhang and J. Zhang, *Chem. Soc. Rev.*, 2015, **44**, 7484–7539.
72 K. M. Abraham, *J. Phys. Chem. Lett.*, 2015, **6**, 830–844.
73 Y. Sun, P. Shi, J. Chen, Q. Wu, X. Liang, X. Rui, H. Xiang and Y. Yu, *Energy Chem.*, 2020, **2**, 100031.
74 M. Zhu, X. Zheng, L. Li, X. Zhu, Z. Huang, G. Wang, Y. Zhang, H. Liu, F. Yu, L. Wen, H.-K. Liu, S.-X. Dou and C. Wu, *Energy Storage Mater.*, 2022, **48**, 466–474.
75 G. Zhang, X. Deng, J. Li, J. Wang, G. Shi, Y. Yang, J. Chang, K. Yu, S.-S. Chi, H. Wang, P. Wang, Z. Liu, Y. Gao, Z. Zheng, Y. Deng and C. Wang, *Nano Energy*, 2022, **95**, 107014.
76 J. Ban, X. Jiao, Y. Feng, J. Xue, C. He and J. Song, *ACS Appl. Energy Mater.*, 2021, **4**, 3777–3784.
77 Y. Zhao, T. Zhou, T. Ashirov, M. E. Kazzi, C. Cancellieri, L. P. H. Jeurgens, J. W. Choi and A. Coskun, *Nat. Commun.*, 2022, **13**, 2575.
78 M. Wu, Z. Wang, W. Zhang, C. Jayawardana, Y. Li, F. Chen, B. Nan, B. L. Lucht and C. Wang, *Angew. Chem., Int. Ed.*, 2023, **62**, e202216169.
79 T. Zhou, Y. Zhao, M. El Kazzi, J. W. Choi and A. Coskun, *Angew. Chem., Int. Ed.*, 2022, **13**, 2575.
80 C.-C. Su, K. Amine, M. Cai and M. He, *ACS Appl. Mater. Interfaces*, 2023, **15**, 2804–2811.
81 H. Lu, Z. Chen, H. Du, K. Zhang, J. Wang, Z. Hou and J. Fang, *Ionics*, 2019, **25**, 2685–2691.
82 Q. Yi, Y. Lu, X. Sun, H. Zhang, H. Yu and C. Sun, *ACS Appl. Mater. Interfaces*, 2019, **11**, 46965–46972.
83 H. Zhang, Z. Zeng, F. Ma, X. Wang, Y. Wu, M. Liu, R. He, S. Cheng and J. Xie, *Adv. Funct. Mater.*, 2023, **33**, 2212000.
84 A. Ramasubramanian, V. Yurkiv, T. Foroozan, M. Ragone, R. Shahbazian-Yassar and F. Mashayek, *ACS Appl. Energy Mater.*, 2020, **3**, 10560–10567.
85 Y. Okuno, K. Ushirogata, K. Sodeyama and Y. Tateyama, *Phys. Chem. Chem. Phys.*, 2016, **18**, 8643–8653.
86 C.-C. Su, M. He, R. Amine, T. Rojas, L. Cheng, A. T. Ngo and K. Amine, *Energy Environ. Sci.*, 2019, **12**, 1249–1254.
87 C. Su, M. He, J. Shi, R. Amine, J. Zhang and K. Amine, *Angew. Chem., Int. Ed.*, 2020, **59**, 18229–18233.
88 Y. Lee, J. Lee, J. Lee, K. Kim, A. Cha, S. Kang, T. Wi, S. J. Kang, H.-W. Lee and N.-S. Choi, *ACS Appl. Mater. Interfaces*, 2018, **10**, 15270–15280.
89 D. R. MacFarlane, N. Tachikawa, M. Forsyth, J. M. Pringle, P. C. Howlett, G. D. Elliott, J. H. Davis, M. Watanabe, P. Simon and C. A. Angell, *Energy Environ. Sci.*, 2014, **7**, 232–250.
90 Q. Yang, Z. Zhang, X.-G. Sun, Y.-S. Hu, H. Xing and S. Dai, *Chem. Soc. Rev.*, 2018, **47**, 2020–2064.
91 D. R. MacFarlane, M. Forsyth, P. C. Howlett, M. Kar, S. Passerini, J. M. Pringle, H. Ohno, M. Watanabe, F. Yan, W. Zheng, S. Zhang and J. Zhang, *Nat. Rev. Mater.*, 2016, **1**, 15005.
92 S. Abada, G. Marlair, A. Lecocq, M. Petit, V. Sauvant-Moynot and F. Huet, *J. Power Sources*, 2016, **306**, 178–192.
93 Y. Yamada and A. Yamada, *J. Electrochem. Soc.*, 2015, **162**, A2406–A2423.
94 K. Xu, *Chem. Rev.*, 2014, **114**, 11503–11618.
95 K. M. Diederichsen, E. J. McShane and B. D. McCloskey, *ACS Energy Lett.*, 2017, **2**, 2563–2575.
96 M. Kar, T. J. Simons, M. Forsyth and D. R. MacFarlane, *Phys. Chem. Chem. Phys.*, 2014, **16**, 18658–18674.
97 A. Lewandowski and A. Świderska-Mocek, *J. Power Sources*, 2009, **194**, 601–609.
98 S. Zhang, J. Sun, X. Zhang, J. Xin, Q. Miao and J. Wang, *Chem. Soc. Rev.*, 2014, **43**, 7838–7869.
99 F. Makhlooghiazad, P. C. Howlett, X. Wang, M. Hilder, D. R. MacFarlane, M. Armand and M. Forsyth, *J. Mater. Chem. A*, 2017, **5**, 5770–5780.
100 M. Forsyth, M. Hilder, Y. Zhang, F. Chen, L. Carre, D. A. Rakov, M. Armand, D. R. Macfarlane, C. Pozo-Gonzalo and P. C. Howlett, *ACS Appl. Mater. Interfaces*, 2019, **11**, 43093–43106.
101 D. A. Rakov, J. Sun, S. A. Ferdousi, P. C. Howlett, A. N. Simonov, F. Chen and M. Forsyth, *ACS Mater. Lett.*, 2022, **4**, 1984–1990.
102 P. M. L. Le, T. D. Vo, H. Pan, Y. Jin, Y. He, X. Cao, H. V. Nguyen, M. H. Engelhard, C. Wang, J. Xiao and J. Zhang, *Adv. Funct. Mater.*, 2020, **30**, 2001151.
103 L. Schafzahl, I. Hanzu, M. Wilkening and S. A. Freunberger, *ChemSusChem*, 2017, **10**, 401–408.
104 Q. Shi, Y. Zhong, M. Wu, H. Wang and H. Wang, *Angew. Chem.*, 2018, **130**, 9207–9210.
105 P. Li, Z. Jiang, X. Huang, X. Lu, J. Xie and S. Cheng, *Nano Energy*, 2021, **89**, 106396.
106 S. Wang, W. Cai, Z. Sun, F. Huang, Y. Jie, Y. Liu, Y. Chen, B. Peng, R. Cao, G. Zhang and S. Jiao, *Chem. Commun.*, 2019, **55**, 14375–14378.
107 H. Wang, C. Zhu, J. Liu, S. Qi, M. Wu, J. Huang, D. Wu and J. Ma, *Angew. Chem.*, 2022, **134**, e202208506.
108 J. Kim, J. Kim, J. Jeong, J. Park, C.-Y. Park, S. Park, S. G. Lim, K. T. Lee, N.-S. Choi, H. R. Byon, C. Jo and J. Lee, *Energy Environ. Sci.*, 2022, **15**, 4109–4118.

109 A. W. Tomich, J. Park, S. Son, E. P. Kamphaus, X. Lyu, F. Dogan, V. Carta, J. Gim, T. Li, L. Cheng, E. Lee, V. Lavallo and C. S. Johnson, *Angew. Chem., Int. Ed.*, 2022, **61**, e202208158.
110 L. Suo, Y.-S. Hu, H. Li, M. Armand and L. Chen, *Nat. Commun.*, 2013, **4**, 1481.
111 Y. Yamada, M. Yaegashi, T. Abe and A. Yamada, *Chem. Commun.*, 2013, **49**, 11194.
112 D. W. McOwen, D. M. Seo, O. Borodin, J. Vatamanu, P. D. Boyle and W. A. Henderson, *Energy Environ. Sci.*, 2014, **7**, 416–426.
113 Y. Yamada, C. H. Chiang, K. Sodeyama, J. Wang, Y. Tateyama and A. Yamada, *ChemElectroChem*, 2015, **2**, 1687–1694.
114 J. Qian, W. A. Henderson, W. Xu, P. Bhattacharya, M. Engelhard, O. Borodin and J.-G. Zhang, *Nat. Commun.*, 2015, **6**, 6362.
115 W. R. McKinnon and J. R. Dahn, *J. Electrochem. Soc.*, 1985, **132**, 364–366.
116 S.-K. Jeong, M. Inaba, Y. Iriyama, T. Abe and Z. Ogumi, *J. Power Sources*, 2008, **175**, 540–546.
117 Y. Yamada and A. Yamada, *J. Electrochem. Soc.*, 2015, **162**, A2406–A2423.
118 J. Wang, Y. Yamada, K. Sodeyama, C. H. Chiang, Y. Tateyama and A. Yamada, *Nat. Commun.*, 2016, **7**, 12032.
119 S.-K. Jeong, H.-Y. Seo, D.-H. Kim, H.-K. Han, J.-G. Kim, Y. B. Lee, Y. Iriyama, T. Abe and Z. Ogumi, *Electrochem. Commun.*, 2008, **10**, 635–638.
120 Y. Yamada, K. Furukawa, K. Sodeyama, K. Kikuchi, M. Yaegashi, Y. Tateyama and A. Yamada, *J. Am. Chem. Soc.*, 2014, **136**, 5039–5046.
121 Y. Yamada, J. Wang, S. Ko, E. Watanabe and A. Yamada, *Nat. Energy*, 2019, **4**, 269–280.
122 Y. Zhao, Y. Bai, Y. Bai, M. An, G. Chen, W. Li, C. Li and Y. Zhou, *J. Power Sources*, 2018, **407**, 23–30.
123 X. Zhang, L. Zou, Y. Xu, X. Cao, M. H. Engelhard, B. E. Matthews, L. Zhong, H. Wu, H. Jia, X. Ren, P. Gao, Z. Chen, Y. Qin, C. Kompella, B. W. Arey, J. Li, D. Wang, C. Wang, J. Zhang and W. Xu, *Adv. Energy Mater.*, 2020, **10**, 2000368.
124 N. Piao, X. Ji, H. Xu, X. Fan, L. Chen, S. Liu, M. N. Garaga, S. G. Greenbaum, L. Wang, C. Wang and X. He, *Adv. Energy Mater.*, 2020, **10**, 1903568.
125 W. Kwak, H. Lim, P. Gao, R. Feng, S. Chae, L. Zhong, J. Read, M. H. Engelhard, W. Xu and J. Zhang, *Adv. Funct. Mater.*, 2021, **31**, 2002927.
126 J. Zheng, S. Chen, W. Zhao, J. Song, M. H. Engelhard and J.-G. Zhang, *ACS Energy Lett.*, 2018, **3**, 315–321.
127 Z. Jiang, Z. Zeng, X. Liang, L. Yang, W. Hu, C. Zhang, Z. Han, J. Feng and J. Xie, *Adv. Funct. Mater.*, 2021, **31**, 2005991.
128 S. Chen, J. Zheng, L. Yu, X. Ren, M. H. Engelhard, C. Niu, H. Lee, W. Xu, J. Xiao, J. Liu and J.-G. Zhang, *Joule*, 2018, **2**, 1548–1558.
129 X. Dong, Y. Lin, P. Li, Y. Ma, J. Huang, D. Bin, Y. Wang, Y. Qi and Y. Xia, *Angew. Chem., Int. Ed.*, 2019, **58**, 5623–5627.
130 J. Zheng, G. Ji, X. Fan, J. Chen, Q. Li, H. Wang, Y. Yang, K. C. DeMella, S. R. Raghavan and C. Wang, *Adv. Energy Mater.*, 2019, **9**, 1803774.
131 H. Jia, L. Zou, P. Gao, X. Cao, W. Zhao, Y. He, M. H. Engelhard, S. D. Burton, H. Wang, X. Ren, Q. Li, R. Yi, X. Zhang, C. Wang, Z. Xu, X. Li, J. Zhang and W. Xu, *Adv. Energy Mater.*, 2019, **9**, 1900784.
132 Y. Jin, Y. Xu, P. M. L. Le, T. D. Vo, Q. Zhou, X. Qi, M. H. Engelhard, B. E. Matthews, H. Jia, Z. Nie, C. Niu, C. Wang, Y. Hu, H. Pan and J.-G. Zhang, *ACS Energy Lett.*, 2020, **5**, 3212–3220.
133 Y. Zheng, F. A. Soto, V. Ponce, J. M. Seminario, X. Cao, J.-G. Zhang and P. B. Balbuena, *J. Mater. Chem. A*, 2019, **7**, 25047–25055.
134 S. Perez Beltran, X. Cao, J.-G. Zhang and P. B. Balbuena, *Chem. Mater.*, 2020, **32**, 5973–5984.
135 J. Zheng, S. Chen, W. Zhao, J. Song, M. H. Engelhard and J.-G. Zhang, *ACS Energy Lett.*, 2018, **3**, 315–321.
136 Y. Jin, Y. Xu, P. M. L. Le, T. D. Vo, Q. Zhou, X. Qi, M. H. Engelhard, B. E. Matthews, H. Jia, Z. Nie, C. Niu, C. Wang, Y. Hu, H. Pan and J.-G. Zhang, *ACS Energy Lett.*, 2020, **5**, 3212–3220.
137 J. Luo, Y. Zhang, E. Matios, P. Wang, C. Wang, Y. Xu, X. Hu, H. Wang, B. Li and W. Li, *Nano Lett.*, 2022, **22**, 1382–1390.
138 X. Zheng, Z. Gu, X. Liu, Z. Wang, J. Wen, X. Wu, W. Luo and Y. Huang, *Energy Environ. Sci.*, 2020, **13**, 1788–1798.
139 R. Jiang, L. Hong, Y. Liu, Y. Wang, S. Patel, X. Feng and H. Xiang, *Energy Storage Mater.*, 2021, **42**, 370–379.
140 S. Wei, S. Choudhury, J. Xu, P. Nath, Z. Tu and L. A. Archer, *Adv. Mater.*, 2017, **29**, 1605512.
141 Y.-W. Byeon, J.-P. Ahn and J.-C. Lee, *Small*, 2020, **16**, 2004868.
142 X. Zheng, H. Fu, C. Hu, H. Xu, Y. Huang, J. Wen, H. Sun, W. Luo and Y. Huang, *J. Phys. Chem. Lett.*, 2019, **10**, 707–714.
143 W. Fang, R. Jiang, H. Zheng, Y. Zheng, Y. Sun, X. Liang, H.-F. Xiang, Y.-Z. Feng and Y. Yu, *Rare Met.*, 2021, **40**, 433–439.
144 J. Chen, Y. Peng, Y. Yin, M. Liu, Z. Fang, Y. Xie, B. Chen, Y. Cao, L. Xing, J. Huang, Y. Wang, X. Dong and Y. Xia, *Energy Environ. Sci.*, 2022, **15**, 3360–3368.
145 Y. Ji, H. Sun, Z. Li, L. Ma, W. Zhang, Y. Liu, L. Pan, W. Mai and J. Li, *J. Mater. Chem. A*, 2022, **10**, 25539–25545.
146 P. Li, Z. Jiang, X. Huang, X. Lu, J. Xie and S. Cheng, *Nano Energy*, 2021, **89**, 106396.
147 P. Li, X. Huang, Z. Jiang, H. Zhang, P. Yu, X. Lu and J. Xie, *Nano Res.*, 2022, **15**, 7172–7179.
148 J. Lee, Y. Lee, J. Lee, S.-M. Lee, J.-H. Choi, H. Kim, M.-S. Kwon, K. Kang, K. T. Lee and N.-S. Choi, *ACS Appl. Mater. Interfaces*, 2017, **9**, 3723–3732.
149 X. Liu, X. Zheng, Y. Dai, W. Wu, Y. Huang, H. Fu, Y. Huang and W. Luo, *Adv. Funct. Mater.*, 2021, **31**, 2103522.
150 F. Ren, Z. Peng, M. Wang, Y. Xie, Z. Li, H. Wan, H. Lin and D. Wang, *Energy Storage Mater.*, 2019, **16**, 364–373.

151 Y. Zhao, L. V. Goncharova, A. Lushington, Q. Sun, H. Yadegari, B. Wang, W. Xiao, R. Li and X. Sun, *Adv. Mater.*, 2017, **29**, 1606663.
152 W. Luo, C. F. Lin, O. Zhao, M. Noked, Y. Zhang, G. W. Rubloff and L. Hu, *Adv. Electrode Mater.*, 2017, **7**, 1601526.
153 V. Kumar, A. Y. S. Eng, Y. Wang, D.-T. Nguyen, M.-F. Ng and Z. W. Seh, *Energy Storage Mater.*, 2020, **29**, 1–8.
154 G. Yang, N. Li and C. Sun, *ACS Appl. Energy Mater.*, 2020, **3**, 12607–12612.
155 D. Li, Y. Sun, M. Li, X. Cheng, Y. Yao, F. Huang, S. Jiao, M. Gu, X. Rui, Z. Ali, C. Ma, Z.-S. Wu and Y. Yu, *ACS Nano*, 2022, **16**, 16966–16975.
156 M. Ma, Y. Lu, Z. Yan and J. Chen, *Batteries Supercaps*, 2019, **2**, 663–667.
157 D. Zhang, B. Li, S. Wang and S. Yang, *ACS Appl. Mater. Interfaces*, 2017, **9**, 40265–40272.
158 V. Kumar, Y. Wang, A. Y. S. Eng, M.-F. Ng and Z. W. Seh, *Cell Rep. Phys. Sci.*, 2020, **1**, 100044.
159 Y. Cheng, X. Yang, M. Li, X. Li, X. Lu, D. Wu, B. Han, Q. Zhang, Y. Zhu and M. Gu, *Nano Lett.*, 2022, **22**, 4347–4353.
160 M. Xu, Y. Li, M. Ihsan-Ul-Haq, N. Mubarak, Z. Liu, J. Wu, Z. Luo and J. K. Kim, *Energy Storage Mater.*, 2022, **44**, 477–486.
161 M. Zhu, G. Wang, X. Liu, B. Guo, G. Xu, Z. Huang, M. Wu, H.-K. Liu, S.-X. Dou and C. Wu, *Angew. Chem.*, 2020, **132**, 6658–6662.
162 Z. Hou, W. Wang, Q. Chen, Y. Yu, X. Zhao, M. Tang, Y. Zheng and Z. Quan, *ACS Appl. Mater. Interfaces*, 2019, **11**, 37693–37700.
163 J. Zhang, S. Wang, W. Wang and B. Li, *J. Energy Chem.*, 2022, **66**, 133–139.
164 H. Fu, Q. Yin, Y. Huang, H. Sun, Y. Chen, R. Zhang, Q. Yu, L. Gu, J. Duan and W. Luo, *ACS Mater. Lett.*, 2020, **2**, 127–132.
165 Y. Cheng, M. Li, X. Yang, X. Lu, D. Wu, Q. Zhang, Y. Zhu and M. Gu, *Nano Lett.*, 2022, **22**, 9614–9620.
166 Z. Gao, J. Yang, H. Yuan, H. Fu, Y. Li, Y. Li, T. Ferber, C. Guhl, H. Sun, W. Jaegermann, R. Hausbrand and Y. Huang, *Chem. Mater.*, 2020, **32**, 3970–3979.
167 S. Zhang, Y. Zhao, F. Zhao, L. Zhang, C. Wang, X. Li, J. Liang, W. Li, Q. Sun, C. Yu, J. Luo, K. Doyle-Davis, R. Li, T. Sham and X. Sun, *Adv. Funct. Mater.*, 2020, **30**, 2001118.
168 F. Colò, F. Bella, J. R. Nair and C. Gerbaldi, *J. Power Sources*, 2017, **365**, 293–302.
169 Y. Li, S. Halacoglu, V. Shreyas, W. Arnold, X. Guo, Q. Dou, J. B. Jasinski, B. Narayanan and H. Wang, *Chem. Eng. J.*, 2022, **434**, 134679.
170 K. Lee, Y. J. Lee, M. J. Lee, J. Han, J. Lim, K. Ryu, H. Yoon, B.-H. Kim, B. J. Kim and S. W. Lee, *Adv. Mater.*, 2022, **34**, 2109767.
171 Z. Xu, Z. Guo, R. Madhu, F. Xie, R. Chen, J. Wang, M. Tebyetekerwa, Y.-S. Hu and M.-M. Titirici, *Energy Environ. Sci.*, 2021, **14**, 6381–6393.
172 Z. Zhang, L. Li, Z. Zhu, Y. Fan, X. Lin, Y. Gu, S. He and Q. Li, *Energy Storage Mater.*, 2022, **53**, 363–370.
173 C. Wei, G. Huang, J. Mao, J. Cai, X. Jin, M. Guan, F. Yu, B. Dai and Y. Li, *ACS Appl. Energy Mater.*, 2022, **5**, 10446–10456.
174 C. B. Soni, V. Kumar and Z. W. Seh, *Batteries Supercaps*, 2022, **5**, e202100207.
175 J. Xia, F. Zhang, J. Liang, K. Fang, W. Wu and X. Wu, *J. Alloys Compd.*, 2021, **853**, 157371.
176 F. Jiang, X. Li, J. Wang, S. Gao, H. Yuan, W. Du, H. Wu, L. Zhu, Y. Hang, Z. Yu, J. Sun and X. Zhang, *J. Alloys Compd.*, 2022, **910**, 164762.
177 Q. Chen, B. Liu, L. Zhang, Q. Xie, Y. Zhang, J. Lin, B. Qu, L. Wang, B. Sa and D.-L. Peng, *Chem. Eng. J.*, 2021, **404**, 126469.
178 C. Bao, J. Wang, B. Wang, J. Sun, L. He, Z. Pan, Y. Jiang, D. Wang, X. Liu, S. X. Dou and J. Wang, *ACS Nano*, 2022, **16**, 17197–17209.
179 X. He, Y. Ni, Y. Li, H. Sun, Y. Lu, H. Li, Z. Yan, K. Zhang and J. Chen, *Adv. Mater.*, 2022, **34**, 2106565.
180 H. Jiang, X. Lin, C. Wei, Y. Zhang, J. Feng and X. Tian, *Small*, 2022, **18**, 2107637.
181 W. Go, M.-H. Kim, J. Park, C. H. Lim, S. H. Joo, Y. Kim and H.-W. Lee, *Nano Lett.*, 2019, **19**, 1504–1511.
182 J. Yan, G. Zhi, D. Kong, H. Wang, T. Xu, J. Zang, W. Shen, J. Xu, Y. Shi, S. Dai, X. Li and Y. Wang, *J. Mater. Chem. A*, 2020, **8**, 19843–19854.
183 B. Tian, Z. Huang, X. Xu, X. Cao, H. Wang, T. Xu, D. Kong, Z. Zhang, J. Xu, J. Zang, X. Li and Y. Wang, *J. Mater. Sci. Technol.*, 2023, **132**, 50–58.
184 S. Ye, F. Liu, R. Xu, Y. Yao, X. Zhou, Y. Feng, X. Cheng and Y. Yu, *Small*, 2019, **15**, 1903725.
185 Z. Zheng, X. Zeng, H. Ye, F. Cao and Z. Wang, *ACS Appl. Mater. Interfaces*, 2018, **10**, 30417–30425.
186 H. Liu, M. Osenberg, L. Ni, A. Hilger, L. Chen, D. Zhou, K. Dong, T. Arlt, X. Yao, X. Wang, I. Manke and F. Sun, *J. Energy Chem.*, 2021, **61**, 61–70.
187 D. Yu, D. Liu, L. Shi, J. Qiu and L. Dai, *J. Mater. Chem. A*, 2021, **9**, 538–545.
188 Z. Tai, Y. Liu, Z. Yu, Z. Lu, O. Bondarchuk, Z. Peng and L. Liu, *Nano Energy*, 2022, **94**, 106947.
189 X. Zheng, W. Yang, Z. Wang, L. Huang, S. Geng, J. Wen, W. Luo and Y. Huang, *Nano Energy*, 2020, **69**, 104387.
190 T.-S. Wang, Y. Liu, Y.-X. Lu, Y.-S. Hu and L.-Z. Fan, *Energy Storage Mater.*, 2018, **15**, 274–281.
191 J. Zhu, J. Yang, J. Zhou, T. Zhang, L. Li, J. Wang and Y. Nuli, *J. Power Sources*, 2017, **366**, 265–269.
192 Q. Lu, X. Wang, A. Omar and D. Mikhailova, *Mater. Lett.*, 2020, **275**, 128206.
193 J. Ni, S. Fu, C. Wu, J. Maier, Y. Yu and L. Li, *Adv. Mater.*, 2016, **28**, 2259–2265.
194 M. Naguib, M. Kurtoglu, V. Presser, J. Lu, J. Niu, M. Heon, L. Hultman, Y. Gogotsi and M. W. Barsoum, *Adv. Mater.*, 2011, **23**, 4248–4253.
195 Y. Fang, R. Lian, H. Li, Y. Zhang, Z. Gong, K. Zhu, K. Ye, J. Yan, G. Wang, Y. Gao, Y. Wei and D. Cao, *ACS Nano*, 2020, **14**, 8744–8753.

196 H. Chen, N. Chen, M. Zhang, M. Li, Y. Gao, C. Wang, G. Chen and F. Du, *Nanotechnology*, 2019, **30**, 134001.
197 H. Jiang, X. Lin, C. Wei, Y. Zhang, J. Feng and X. Tian, *Small*, 2022, **18**, 2107637.
198 J. Luo, C. Wang, H. Wang, X. Hu, E. Matios, X. Lu, W. Zhang, X. Tao and W. Li, *Adv. Funct. Mater.*, 2019, **29**, 1805946.
199 Y. Zhang, F. Wu, Y. Huang, S. Li, C. Li, Z. Wang and M. Xie, *J. Mater. Chem. A*, 2022, **10**, 11553–11561.